Report
R-23-19
December 2024

Site scale modelling of groundwater evolution at SFR

A modelling application with iDP

Gabriela Román-Ross
Aitor Iraola
Paolo Trinchero
Jorge Molinero

SVENSK KÄRNBRÄNSLEHANTERING AB

SWEDISH NUCLEAR FUEL
AND WASTE MANAGEMENT CO

Box 3091, SE-169 03 Solna
Phone +46 8 459 84 00
skb.se

SVENSK KÄRNBRÄNSLEHANTERING

ISSN 1402-3091
SKB R-23-19
ID 1615694

December 2024

Site scale modelling of groundwater evolution at SFR

A modelling application with iDP

Gabriela Román-Ross, Aitor Iraola,
Paolo Trinchero, Jorge Molinero

Amphos 21, Consulting S.L.

Keywords: SFR, Modelling, Hydrogeochemical evolution.

This report concerns a study which was conducted for Svensk Kärnbränslehantering AB (SKB). The conclusions and viewpoints presented in the report are those of the authors. SKB may draw modified conclusions, based on additional literature sources and/or expert opinions.

This report is published on www.skb.se

© 2024 Svensk Kärnbränslehantering AB

Abstract

The chemical composition of groundwater around a repository for radioactive waste depends on many processes that simultaneously involve groundwater flow, transport and chemical reactions. Thus, the reliable characterization of a rock volume candidate site for a repository should be based on coupled numerical approaches able to integrate hydrogeology and hydrochemistry. However, mainly due to numerical and conceptual constraints and the computational requirements, most studies have treated the key processes separately. The present study was developed with the aim to improve the integration of hydrogeology and geochemistry in a 3D reactive model implemented for describing the evolution of the geosphere surrounding the SFR repositories. Calculations were performed with iDP (interface DarcyTools-PFLOTRAN). This interface, owned by SKB and developed by Amphos 21, is a versatile tool that provides a large range of abilities to represent processes occurring in the geosphere at different scales. Output options permit the selection of chosen chemical species and minerals at specified locations and times for analysis and visualization, both in fracture and rock matrix domains.

Processes linked to the rock matrix have been implemented by using the multi-continuum approach developed by Lichtner et al. (2013) and included in the PFLOTRAN software. Several validation tests were carried out before adding the reactive rock matrix domain in the 3D models. All these tests are detailed in this report.

The 3D reactive transport calculations have been run for the same geochemical cases defined in previous models performed with FASTREACT (Román-Ross et al. 2014). The Base Case assumes local equilibrium conditions with calcite/hematite and the alternative geochemical case (Variant Case) has been computed in equilibrium with calcite/amorphous iron monosulphide (FeS(am)). The numerical simulations reproduce the interactions between the fracture groundwater and the rock matrix during a time span of 3 500 years (from 2500 AD to 6000 AD) taking into account the ongoing shoreline displacement and the increasing influence of altered meteoric water over time at the Forsmark site.

The obtained results with the 3D models have been compared with those previously computed with FASTREACT (Román-Ross et al. 2014) obtaining a good agreement with the models run without reactive matrix.

Our results show that rock matrix could have a relevant role in the attenuation of abrupt chemical changes (i.e infiltration of meteoric waters due to land uplift) and need to be included in the geochemical models. The main challenge remains to adequately parameterize this very heterogenous domain.

Coupled reactive transport calculations are now feasible at site scale for the SFR repositories computing hydrogeological and hydrogeochemical processes in a site descriptive model that also integrates topography, which is prescribed as upper boundary of the model. These 3D models provide a framework for implementing more complex applications in the future.

Sammanfattning

Den kemiska sammansättningen av grundvattnet kring ett förvar för radioaktivt avfall beror på många processer som samtidigt inbegriper grundvattnets flöde, ämnestransport och kemiska reaktioner. Pålitlig karakterisering av bergvolymkandidater för slutförvar bör således baseras på kopplade numeriska metoder som kan integrera hydrogeologi, hydrogeokemi. På grund av numeriska och konceptuella begränsningar samt krav på beräkningsresurser, har de flesta studier behandlat de viktiga processerna separat. Föreliggande studie har utvecklats med syftet att förbättra integrationen av hydrogeologi och geokemi i en 3D reaktiv modell för att beskriva utvecklingen av geosfären kring SFR förvaren. Beräkningarna utfördes med iDP (gränssnitt DarcyTools-PFLOTRAN). Detta gränssnitt, ägt av SKB och utvecklats av Amphos 21, är ett högpresterande verktyg som har omfattande utbud av tillvägagångsätt för att representera processer som sker i geosfären i olika skalor. Utdatahanteringen tillåter val av olika utvalda kemiska ämnen och mineraler på angivna platser och tider för både analys och visualisering, i sprickor och bergmatrisdomäner.

Processer kopplade till bergmatrisen har implementerats genom tillämpning av ett multikontinuum, enligt metoden utvecklad av Lichtner et al. (2013) och har inkluderats i programvaran PFLOTRAN. Flera verifieringstester genomfördes innan domänen med reaktiv bergmatris lades till i 3D-modellen. Alla dessa tester redovisas i denna rapport.

Beräkningarna av 3D reaktiva transport har gjort för samma geokemiska fall som definieras i tidigare modeller med FASTREACT (Román-Ross et al. 2014). Basfallet förutsätter villkor uppfyllda för lokal jämvikt med kalcit/hematit och i det alternativa Variant fallet har geokemin beräknats under rådande jämvikt med kalcit/FeS(am). De numeriska simuleringarna reproducera samspelet mellan grundvattnet i sprickor och bergmatrisen under en tidsperiod på 3 500 år (från 2500 AD till 6000 AD) med hänsyn till den då pågående strandlinjeförskjutningen samt den ökande påverkan av infiltrerande meteoriskt vatten över tid i Forsmark.

De erhållna resultaten med de 3D-modellerna har jämförts med de tidigare resultaten beräknats med FASTREACT (Román-Ross et al. 2014) och en god överrensstämmelse har erhållits för modellerna som inte har reaktiv bergmatris.

Våra resultat visar att bergmatrisen skulle kunna ha en relevant roll i dämpningen av abrupta kemiska förändringar (infiltration av meteoriskt vatten pga landhöjningen) som behöver tas hänsyn till i de geokemiska modellerna. Den största utmaningen förblir adekvat parameterisering av denna mycket heterogena bergdomän.

Kopplade reaktiva transportberäkningar är nu genomförbara i platsskala för SFR förvaren, som simulerar hydrogeologiska samt hydrogeokemiska processer i en platsbeskrivande modell som även integrerar topografi, vilket utgör övre gränsen för modellen. Dessa 3D-modeller utgör ett ramverk som möjliggör beräkningar av mer komplexa applikationer i framtiden.

Notation

Parameter	Name	Units
p(z)	Hydrostatic pressure	Pa
p_0	Reference pressure	Pa
ρ	Water density	kg/m^3
g	Gravity	m/s^2
v_{flux}	Velocity of flux	m/day
ϵ_f	Fracture volume fraction	[-] adimensional
δ	Half fracture aperture	m
A_{fm}	Fracture-matrix specific surface	m^{-1}
τ	Tortuosity	[-] adimensional
D_0	Diffusion coefficient in free water	m^2/s
D_p	Pore diffusion coefficient	m^2/s
ϕ_m	Matrix porosity	[-] adimensional
D^{eff} (= τD^*)	Effective diffusion coefficient	m^2/s
R'	Matrix retardation coefficient	[-] adimensional
λ	Decay constant	1/s
c	Solute concentration	mol/L
D^0	Molecular diffusion coefficient	m^2/s
ρ_b	Bulk density of the matrix	kg/m^3
K_f	Distribution coefficient	m
v	Water velocity	m/day
R	Fracture retardation coefficient	[-] adimensional
D	Fracture hydrodynamic dispersion coefficient	m^2/s
θ	Matrix porosity (as in Tang et al. 1981)	[-] adimensional

Contents

1 Introduction 9
1.1 Background 9
1.2 Scope and structure of the report 10

2 Model set-up 11
2.1 Theoretical background 11
2.2 Input data from the DarcyTools model 11
2.3 Geometrical simplification 13
  2.3.1 Geometry and mesh 14
  2.3.2 Initial and boundary conditions for flow 16
  2.3.3 Initial and boundary conditions for reactive transport 20

3 Rock matrix diffusion 23
3.1 Model description 23
  3.1.1 1D model 23
  3.1.2 2D model 24
  3.1.3 Analytical resolution 25
3.2 Verification tests 26
3.3 Matrix diffusion verification under reactive conditions 27
  3.3.1 Nested cubes approach 29
3.4 Verification example applied to the SFR repository 31
  3.4.1 Numerical model 31
3.5 Implementation of the multicontinuum approach into the 3D model 33
  3.5.1 Flow velocity issue 33
  3.5.2 Unsaturated flow 34

4 3D model with reactive matrix 35

5 Concluding remarks and further work 43

References 45

Appendix 47

1 Introduction

1.1 Background

The Swedish Nuclear Fuel and Waste Management Company (SKB) is going to build the extension of the final repository for low and medium level radioactive operational waste, SFR in Forsmark. The SFR facility is located in northern Uppland close to the Forsmark nuclear power plant within about 120 km north of Stockholm in a crystalline rock environment. The area forms part of a crustal segment in the Fennoscandian Shield. The strongly deformed rocks in the SFR area is mainly composed of intermediate metavolcanic rocks intercalated with biotite-bearing metagranodiorite (to granite) types (Curtis et al. 2011). The existing facility, denominated SFR1, is covered by 60 m of granitoid rocks while the proposed extension, SFR3, is planned at 120 m depth under the seabed (SKB, 2014). As mentioned in several SKB reports (Trinchero et al. 2014, Joyce et al. 2015, Molinero et al. 2016), reliable characterization of candidate sites for the location of geological repositories, requires integration of hydrogeology and geochemistry in the reactive transport models. Despite large efforts made by SKB over the last decades to make this possible integration, more studies and computational resources are needed to satisfy the requirements for such an integration. For a more exhaustive integration beyond the conceptual level, developing and implementing numerical codes able to adequately represent the mutual influence of the hydrogeological and geochemical processes are needed. Main efforts were devoted to solve these constraints by implementing a full 3D reactive transport model able to provide a confident coupled approach for future application within safety assessment scenarios.

In a previous work, the evolution of groundwaters in the host-rock surrounding the SFR repositories (i.e. the currently emplaced repository SFR1 and the future extension SFR3) was modelled using the FASTREACT approach (Trinchero et al. 2014, Román-Ross et al. 2014), which is based on the theory of Stochastic-Convective (SC) models (Shapiro and Cvetkovic 1988). These models rely on the assumption that local-scale dispersion can be neglected and flow is steady. The infiltration occurs in an extended and complex network of deformation zones and fractures in which the infiltrating waters (i.e. boundary waters), react with the rock and fracture filling minerals. Mass exchange between the transmissive zones and the low permeable rock matrix was simulated using a dual porosity approach (Román-Ross et al. 2014). This approach allows to mimic interactions between the "mobile" domain (i.e. deformation zones and fractures with relatively high hydraulic conductivity) and the low-conductive matrix. The dual porosity representation of the fractured medium consists of two continua (i.e. matrix and fractures), which are described by a parallel fracture model. At that time, this methodology was implemented as an alternative to site-scale three-dimensional reactive transport models which are computationally expensive due to their large number of degrees of freedom and the underlying system of non-linear partial and ordinary differential equations. By decomposing these 3D problems in sets of 1D calculations, the computational burden is reduced dramatically, and the numerical analyses can efficiently be handled in standard powerful workstations.

The technological constraints for the use of three-dimensional reactive transport models have been overcome by using the "DarcyTools-PFLOTRAN interface" (iDP). This interface, developed by Amphos 21 (Molinero et al. 2016) and owned by SKB, combines two powerful codes:

1. DarcyTools (Svensson et al. 2010) is a computer code for the simulation of flow and transport in subsurface heterogeneous media. The code, which has been developed for more than 15 years by MFRDC (Michel Ferry R& D Consulting) and CFE AB (Computer-aided Fluid Engineering AB), has been used in the Swedish and Finnish safety analyses SR-Site and TURVA2012. One of the added values of DarcyTools is the capability of simulating flow and transport processes in fractured crystalline rocks.
2. PFLOTRAN (Hammond et al. 2014) is an open source, massively parallelized flow and reactive transport code that has been developed for calculation in high performance computing (HPC) environments. PFLOTRAN which has been under active development and improvement by a group of researchers, most of them working at Sandia National Laboratory, Los Alamos National Laboratory, Pacific Northwest National Laboratory, Oak Ridge National Laboratory and Lawrence Berkeley National Laboratory. In addition, IDP has been successfully tested on two "big" (large-

scale, computationally demanding) application cases solved in two different "big" (powerful) supercomputers and verified against well-known benchmark problems, constitutes a breakthrough technology for future SKB applications (Molinero et al. 2016).

By applying this methodological approach, a 3D reactive transport model was developed for the SFR repository including matrix diffusion. Geosphere surrounding the SFR repositories was conceptualized as an upscaled equivalent continuous porous medium (ECPM). The heterogeneous properties (i.e. the permeability field and pressure boundary conditions) of the ECPM were computed by DarcyTools and converted to PFLOTRAN using iDP. The interaction between the flowing water in fractures and the porous rock matrix is quantified by implementing the multicontinnum approach (Lichtner 2000) that allows a flexible discretisation of the reactive rock matrix. The model integrates hydrogeological models with the most relevant site-specific reactive transport processes. This integration aims at capturing the mutual interdependence of flow and groundwater chemical patterns.

1.2 Scope and structure of the report

This work focuses on the implementation and validation of a reactive matrix formulation in a 3D site-scale model using a reactive transport approach for the analysis of the evolution of groundwaters at SFR. The model integrates shoreline displacement, chemical interactions between groundwaters and fracture filling minerals and a reactive rock matrix domain. The effect of reactive rock matrix was assessed through a comparison with previous calculations performed using FASTREACT (Román-Ross et al. 2014).

The models simulate the evolution of groundwater composition during a time span of 3 500 years (from 2500 AD to 6000 AD). This choice is based on the assumption that no major geochemical changes occur in the first 500 years (i.e. from 2000 AD to 2500 AD). Calculations start at 2500 AD and during the whole simulation, a meteoric water infiltrates and progressively penetrates along the recharge paths. The regional-scale-modelling methodology is performed using iDP (interface DarcyTools-PFLOTRAN, Molinero et al. 2016) and the geochemical conceptual models described in Román-Ross et al. (2014). In the reactive transport calculations denoted as "Base Case" calcite and hematite are assumed to be under local equilibrium constraints. Sensitivity analysis considers one Variant Case where equilibrium conditions with FeS(am) are imposed instead of hematite. A more detailed description of the geochemical model is presented in Section 2.3.3.

The full 3D model includes the coupled effects of groundwater flow, and chemical reactions including a reactive rock matrix domain. The interactions between the fracture groundwater and the rock matrix where implemented with the multicontinuum approach developed by Lichtner (2000) and included in the PFLOTRAN software. In addition to these numerical constraints, the topography of the island is prescribed as upper boundary of the model.

After briefly introducing the scientific and methodological framework of the present study (Chapter 1), the model setup is widely described and validated in Chapter 2. Chapter 3 contains the discussion of the results obtained for some selected key parameters. Chapter 4 is aimed to provide a summary of main conclusions and future applications.

2 Model set-up

2.1 Theoretical background

The model reported here was implemented using iDP. A detailed description of the software capabilities can be found in Molinero et al. (2016). As a summary, iDP is the interface between DarcyTools[1] v. 3.5 and PFLOTRAN[2] (v. 95c4fa0). The iDP tool allows the user to read a sub-domain from the DarcyTools flow simulation and export it in a suitable format for PFLOTRAN. In the iDP framework, the groundwater flow equation is first solved by DarcyTools, this result is extracted using iDP and PFLOTRAN input files are generated. In the last step, PFLOTRAN reads the flow solution and performs the reactive transport simulation. The output files are postprocessed with Paraview v. 5.0 (Ahrens et al. 2005), an open source code optimised for multi-platform data analysis and visualization.

Groundwater transport is dominated by advection in fast flowing channels in fractures and fracture zones in the rock. In general terms, the model accounts for dissolved species in flowing groundwater, interacting with the fracture filling minerals and the porous rock matrix. Explicit longitudinal/transversal dispersion is not considered in the flow model.

In this chapter, the main steps taken to build the hydrogeochemical model and run the simulations are summarized.

2.2 Input data from the DarcyTools model

The PFLOTRAN model is initialized with the information provided by the DarcyTools simulations (see Appendix). Table 2-1 describes the input data delivered by SKB for three different time steps corresponding to the DarcyTools simulation times. The considered flow and transport parameters are directly applied at the specified times, with no interpolation in between. Flow conditions are quite heterogeneous and slow during the first 500 years (2000–2500 AD). From 2500 AD onward, travel times become very short and hydrogeological parameters are updated at this time. From 3000 AD the system reaches quasi steady-state conditions and no major changes occur. A more detailed description of the hydrogeological model can be found in Román-Ross et al. (2014).

Table 2-1. Input data taken from the DarcyTools model.

Times (AD)		
2500	**3500**	**5000**
Permeability values	Permeability values	Permeability values
Porosity values	Porosity values	Porosity values
Pressure values	Pressure values	Pressure values

The following assumptions were considered for the initial data:

1. Permeability is kept constant over time, in consequence, only the values corresponding to 2500 AD are taken into account.
2. Flow boundary conditions are built from pressure values and applied to the top, bottom and side boundaries of the model.

The sketch shown in Figure 2-1 illustrates the methodological approach implemented to read the DarcyTools binary files and obtain datasets within the PFLOTRAN sub-domains.

---

[1] DarcyTools is a computer code for simulation of flow and transport in porous and/or fractured media.

[2] PFLOTRAN is an open source, state-of-the-art massively parallel subsurface flow and reactive transport code.

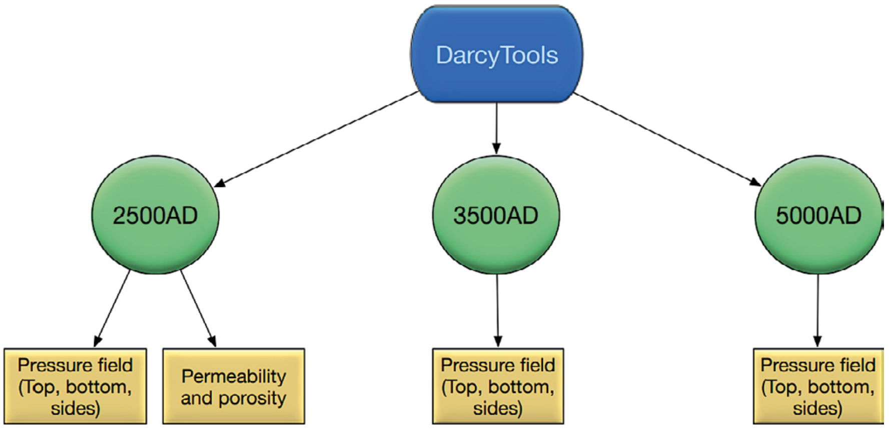
DarcyTools
2500AD
3500AD
5000AD
Pressure field (Top, bottom, sides)
Permeability and porosity
Pressure field (Top, bottom, sides)
Pressure field (Top, bottom, sides)

Figure 2-1. Overview of the iDP-DT set-up showing the start and restart time steps.

The initialization steps for the iDP model can be seen in Figure 2-2. The first step is to generate the geometry and the unstructured mesh of the model. This is done using a powerful pre- and post-processor denoted as GiD (https://www.gidhome.com/), which has been developed by CIMNE (International Center for Numerical Methods in Engineering) and makes it possible to generate complex geometries and unstructured meshes.

iDP is used to extract the DarcyTools (from now on DT) result files (*i.e.* the .rof files) that contain the permeability and pressure data.

The extracted rof files are then interpolated into the PFLOTRAN mesh. This procedure is twofold: on one hand, a trilinear interpolation is performed over the permeability dataset and the unstructured grid of the model. This interpolation allows upscaling of the DarcyTools permeability into the PFLOTRAN mesh. On the other hand, the pressure dataset is interpolated at the boundaries of the model. Specifics of this latter procedure are explained in Section 2.3.2.

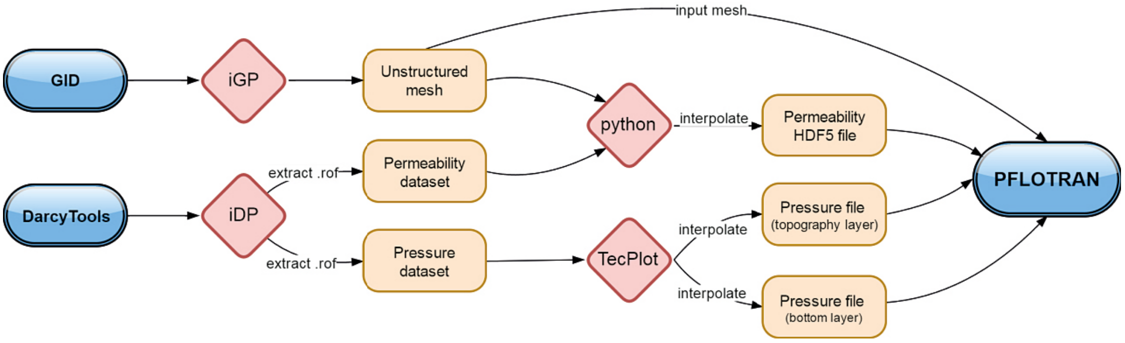
input mesh
GID
iGP
Unstructured mesh
python
interpolate
Permeability HDF5 file
PFLOTRAN
extract .rof
Permeability dataset
DarcyTools
iDP
Pressure file (topography layer)
interpolate
extract .rof
Pressure dataset
TecPlot
interpolate
Pressure file (bottom layer)

Figure 2-2. Diagram showing the programs used and the main modelling steps taken to run the simulations.

2.3 Geometrical simplification

The size of the raw DT data is large (*i.e.* it contains more than 10^6 nodes) and has a very irregular geometry on the boundaries. This makes the geometry and mesh generation computationally inefficient (i.e. the spatial discretization needs to be very fine to fit the mesh to the original model boundaries). To deal with this issue, a geometrical simplification of the DT model has been performed as the first modelling step.

Figure 2-3 shows the selected model domain imbedded into the whole DT region. This simplification allows generating an unstructured grid with 300 000 nodes approximately which improves the modelling capabilities. This is particularly relevant for implementing topography fields and/or the multicontinuum approach to simulate the rock matrix.

The extension of the new geometry is reduced approximately by one half and it is now focused around the repository area. The shoreline at 2500 AD separates the model in two regions that will later be used to apply specific boundary conditions that model the overtime rise of the shoreline and the consequent submergence of the region. The irregular edges present in the DT model are approximated with straight lines in order to simplify the meshing process.

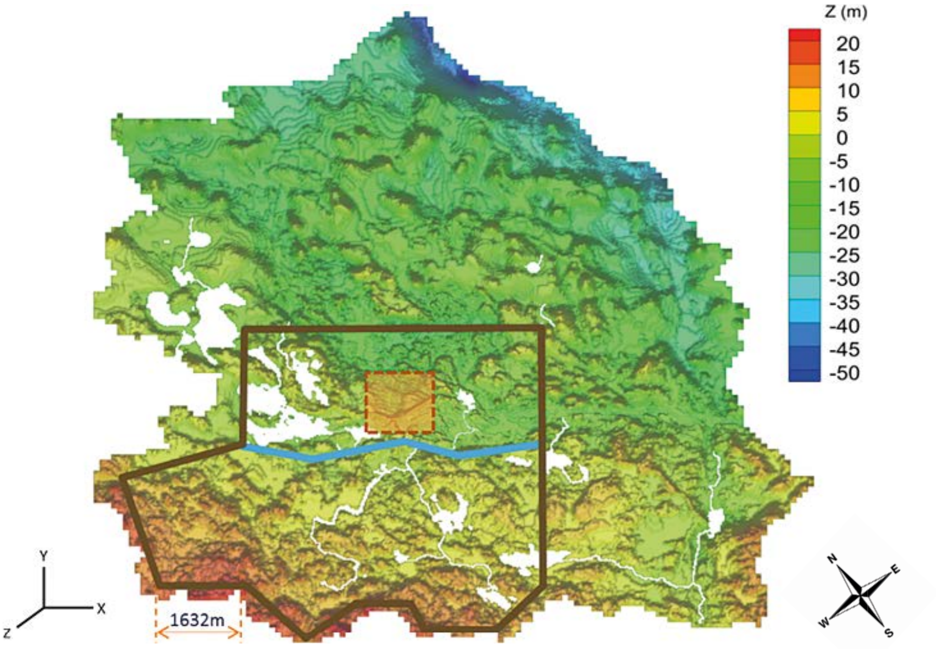

Figure 2-3. *The simplified model (thick brown line) imbedded into the DT region. The lighter zone inside the simplified model is used to set a finer refinement close to the repository area as shown in Figure 2-4. The shoreline at 2500 AD is drawn in blue and the repository site in light brown.*

2.3.1 Geometry and mesh

Geometry

Besides allowing the generation of complex geometries and meshes, GiD has the capability to create customized add-ons. In particular, we used a customised application called iGP (GiD-PFLOTRAN interface, Iraola 2015) that allows the user creating and exporting the geometry, boundary conditions and meshing directly into the PFLOTRAN input format.

As stated in the previous section, the geometry of the model has been simplified. Figure 2-4 shows the layout of the model where there are two main region blocks separated by the shoreline (region “a” on the one hand and regions “b” and “c” on the other hand). The northern region has a small subregion (region “c”) surrounding the repository area that allows to build a variably refined mesh (i.e. a mesh that will be highly refined close to the repository).

Once the layout of the model has been defined, the top layer has been replaced with the topography layer taken from the Darcy Tool model. Figure 2-5 shows the input points that have been used to build the topography surface. This set of points represents the uppermost region of the DT model and it is labelled as “HSD_surface”. Notice that region “c” in Figure 2-4 lays inside the highly refined zone shown in Figure 2-5 (i.e. the lighter zone close to the top right corner), which is the zone where the repository is located.

It should be noted that a more refined zone was defined around the repository area.

GiD has the capability to parameterize a given set of points into a NURBS (Non-uniform rational B-spline) surface. A NURBS surface is a spline based mathematical object that can describe a 2D surface parametrically. It is particularly useful to interpolate a set of points into a regular and smooth surface. This interpolation can be further refined until the desired smoothness is obtained. Thus, this technique allows us to improve the meshing process of the topography data by smoothing the rough edges that would otherwise be found on the point-based dataset. GiD allows to control the smoothing of the created NURBS surface. In this work, however, the smoothing factor has been accommodated to create a computationally efficient mesh. Due to this, there is not an exact, 1 to 1 equivalence between the topography points and the top boundary of the mesh. However, the smoothed surface captures the main and most relevant changes in topography.

As shown in Figure 2-6, the next step is to intersect the boundaries of the model with the NURBS surface that contains the topography. To do so, the GiD model’s boundaries are extruded and intersected with the topography NURBS surface. Later, the exceeding part of these extruded surfaces is deleted and the inner intersected surface is kept. The intersected surface has the variation of the topography while keeping the dimensions and regions of the model (a, b and c).

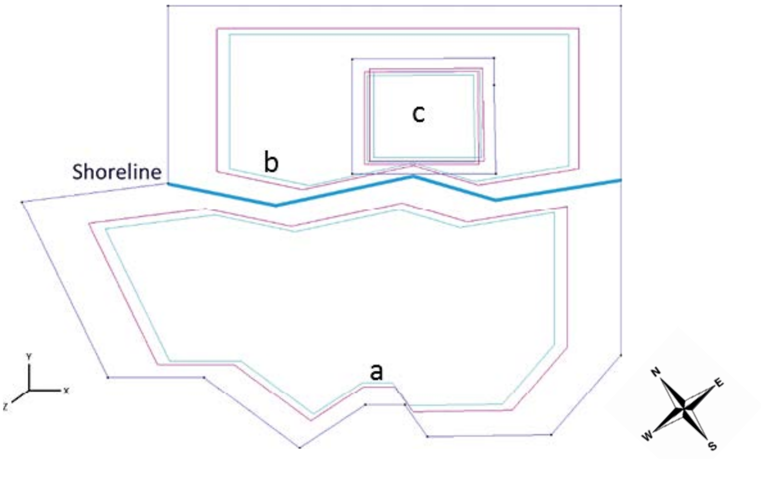

Figure 2-4. *Top view of the geometry (GiD). Notice the aforementioned three regions: a at the southern part of the shoreline, b north of the shoreline and c inside region b. The region c is used to set a finer refinement close to the repository area.*

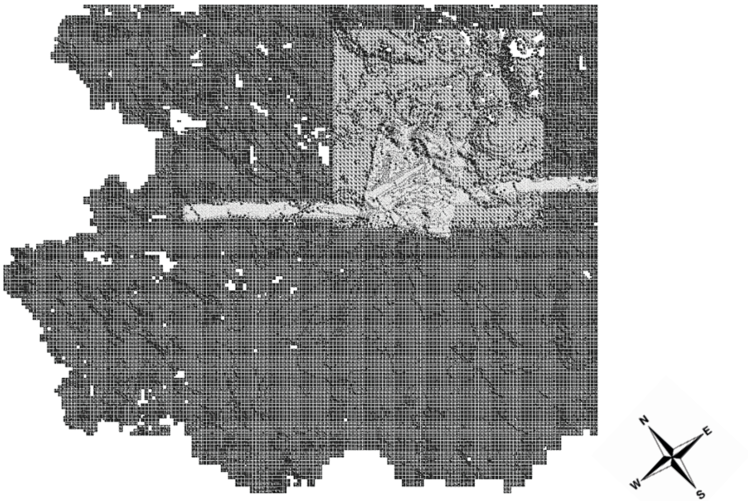

Figure 2-5. *Cloud of points of the HSD_surface on GiD. Notice that the points are not regularly spaced. Due to this, a higher density of points is shown at the top right zone, close to the repository area. This causes a visualization artifact that lightens that zone.*

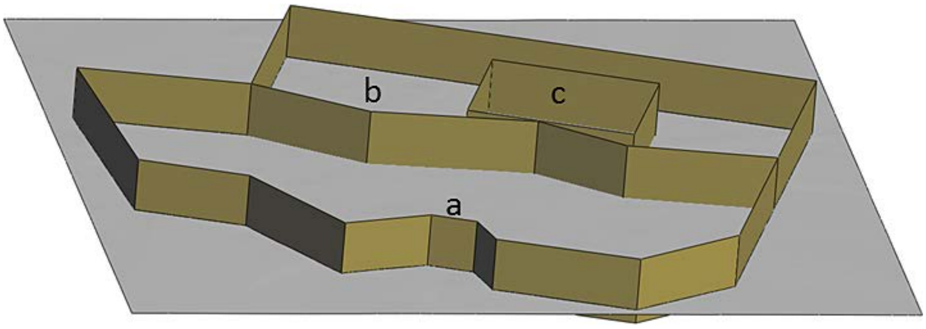

Figure 2-6. *Extrusion of the model lines to intersect the NURBS topography layer. The extruded lines are deleted and the inner surfaces are kept.*

Once the surface layer is set-up in the model, two different 3D volumes are created by extrusion. One layer for the surface region ($z \in [-20, z_{topography}]$), and the other for the underground region ($z \in [-200, -20]$). This allows us to easily and adequately adopt the meshing to the purpose of the model. For instance, the surface region could be refined to improve the spatial resolution for modelling processes occurring in the biosphere (Figure 2-7a).

To improve visualization, the model shown in the figures has the z coordinate exaggerated by a factor of 25 in the topography region ($z \in [-20, z_{topography}]$) and by a factor of 4 in the underground region (Figure 2-7a). Figure 2-7b represents the final geometry of the model.

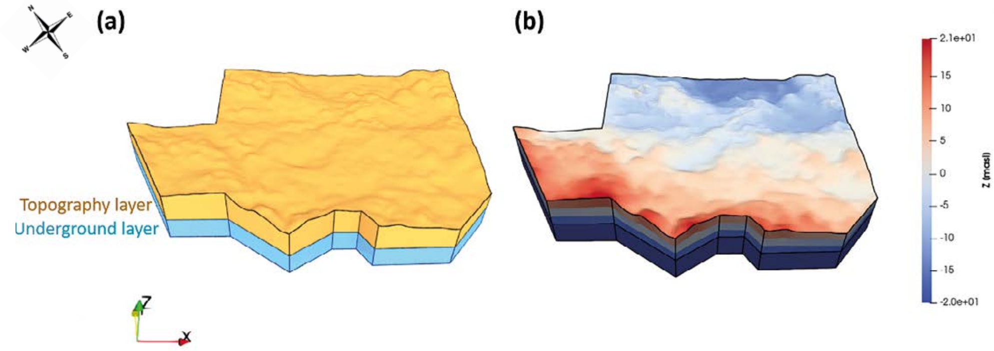

Figure 2-7. *Geometry of the model.*

Mesh

A semi-structured prismatic mesh (also known as a “layered mesh”) was implemented in the model. This kind of mesh is unstructured in the XY plane but structured, and layer based, in the Z direction. Even though completely unstructured meshes offer a better efficiency regarding the number of total elements, they typically show distorted elements that can affect the convergence of the models. This issue is especially relevant in the case of PFLOTRAN since it is based on a first-order spatial discretization. In contrast, semi-structured meshes offer a great balance between versatility to mesh complex regions and quality of the generated elements.

Figure 2-8 represents the mesh that has been used in the model. The average size of the elements outside of the repository area is 85 m and they are progressively refined up to 30 m in the region closer to the repository.

To define a semi-structured mesh, the total number of layers for each region needs to be provided. The mesh used in the model has 15 layers, which are distributed in the following way: the surface region has been assigned 3 layers, and the rest are part of the deeper region (12 layers). This results in a constant spatial discretization in the underground region (i.e. because the top and bottom layers are flat) that has a value of dz = 15 m. However, when topography is added, the top surface becomes uneven, resulting in a variable spatial discretization along the z-axis. This variable discretization has a lowest value of dz = 1.73 m, which occurs in the shallowest zones of the topography, and a highest value of dz = 13.59 m, which happens when the width of the model is high. Figure 2-8 shows a side and top view of the model’s mesh.

Figure 2-8c represents the thin layer that can be found in the uppermost part of the mesh. This layer has a width of 1 m and it is used to properly set the boundary conditions at the topography layer.

2.3.2 Initial and boundary conditions for flow

Permeability

The permeability field of the model comes from the DT data delivered by SKB (see Section 2.2). After extracting the data using iDP, a python script linearly interpolates the data into the PFLOTRAN mesh. Figure 2-9 displays the x-component value of the anisotropic permeability field.

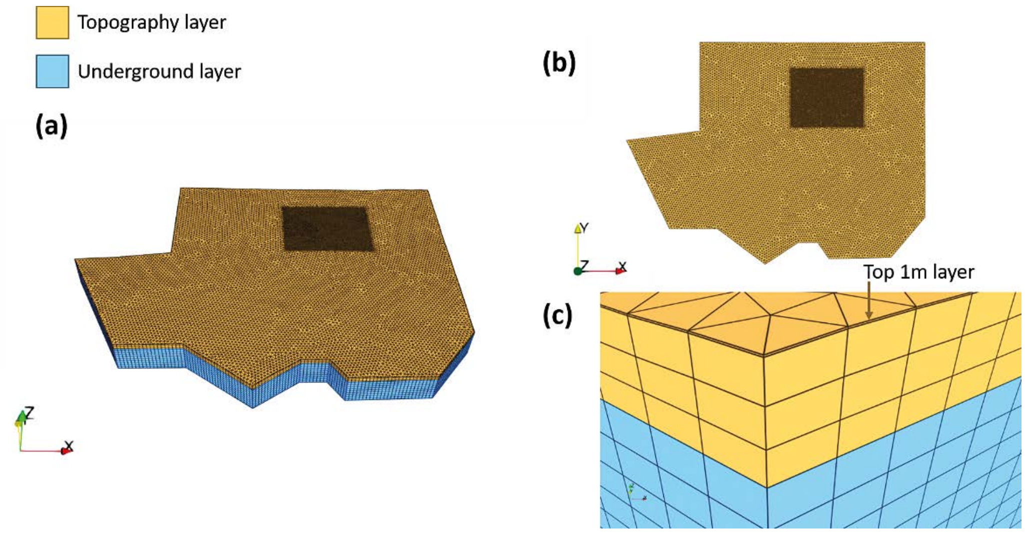

Figure 2-8. *(a) Side and (b) top views of the model mesh, c: side view focused on the top 1 m layer.*

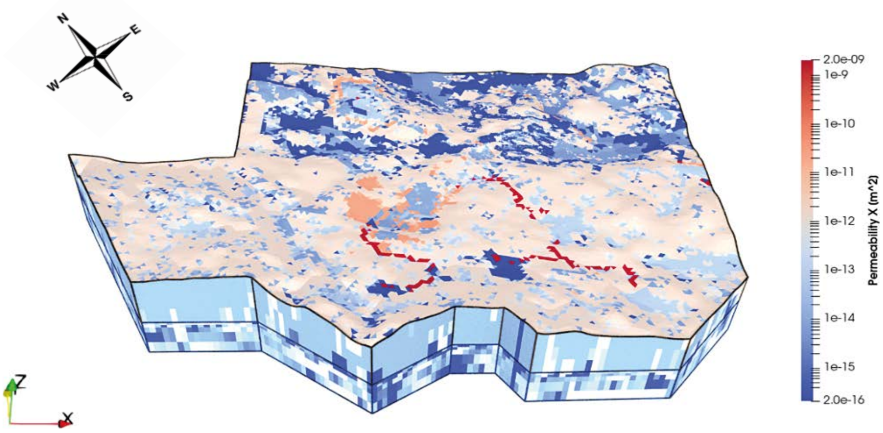
N
E
W
S
2.0e-09
1e-9
1e-10
1e-11
1e-12
1e-13
1e-14
1e-15
2.0e-16
Permeability X (m^2)
Z
X

***Figure 2-9.** The x-component of the permeability field.*

Pressure

A Dirichlet pressure boundary condition (i.e. a fixed value boundary condition) on applied in the top and the bottom layers of the model using the pressure field that comes from the DT model.

PFLOTRAN does not allow a boundary condition to be assigned in a cell-by-cell manner. Thus, the pressure field cannot be interpolated externally into the boundary region of the mesh. However, PFLOTRAN allows loading a cartesian regular grid that contains a given variable data, and it is able to internally interpolate it into the mesh. This kind of interpolation is known by PFLOTRAN as a gridded dataset interpolation. This latter approach has been used to apply the flow boundary conditions in our model.

When a layer is flat, the methodology is rather simple to implement. In summary, a cartesian plane (at $z = -200$ m) is built around the DT model and the pressure field is extracted using iDP. Then, this cartesian grid is converted into HDF5 (i.e. the binary file format used in PFLOTRAN to import/export data) and imported into PFLOTRAN as a gridded dataset. PFLOTRAN will then interpolate the data into the mesh centroids automatically.

However, when the layer is not flat (e.g. in the topography layer) the approach is slightly different. First, the centroids that lay on the topography (i.e. in the top 1 m layer) need to be extracted, and the DT pressure is interpolated on them. This data is then projected into a 2D cartesian grid and imported to PFLOTRAN. The key point here is that PFLOTRAN assigns gridded datasets directly into the selected boundary region. So, even though the 2D grid does not have any information about the elevation, the mesh does, and the methodology properly applies the boundary pressure in the top surface layer, following the topography of the model. A qualitative and quantitative analysis of the pressure interpolation at 2500 AD and 3500 AD, respectively, are shown in Figures 2-10, 2-11, 2-12 and 2-13.

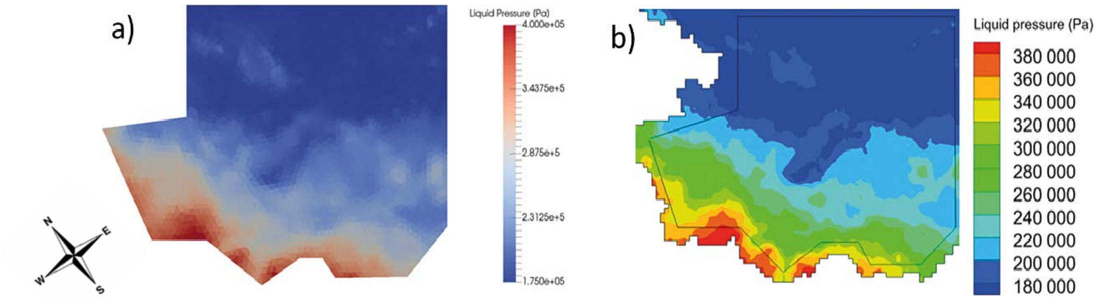
a)
Liquid Pressure (Pa)
4.000e+05
3.4375e+5
2.875e+5
2.3125e+5
1.750e+05
N
E
W
S
b)
Liquid pressure (Pa)
380 000
360 000
340 000
320 000
300 000
280 000
260 000
240 000
220 000
200 000
180 000

***Figure 2-10.** Qualitative comparison of pressures at the top layer (t = 2500 AD) for both the PFLOTRAN model and the DT model.*

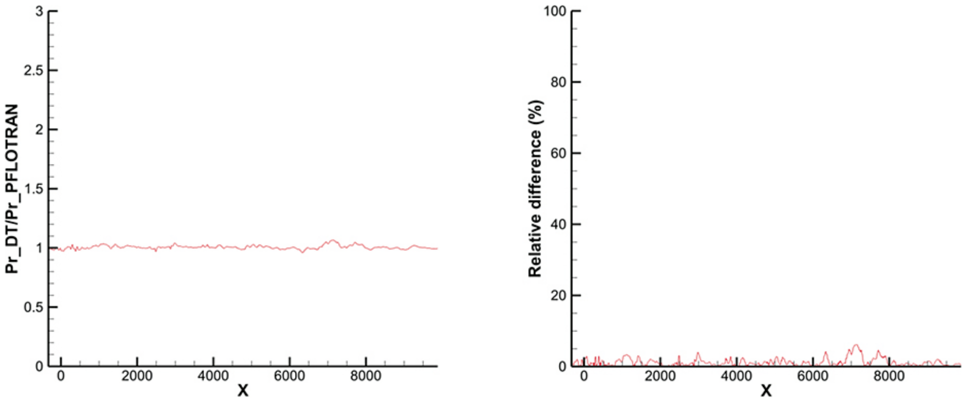

Figure 2-11. *Quantitative comparison of pressures over the line: x ∈ [−328, 9880], y = 8640, z = −20 m at t = 2500 AD. The plot intends to compare the quality of the interpolation between the DT and PFLOTRAN models. The plot shows the quotient* $Dif=\frac{p_{DT}}{p_{PFLOTRAN}}$ *and the relative pressure difference* $(RPD=\left|\frac{p_{DT}-p_{PFLOTRAN}}{p_{DT}}\right|\cdot 100\ (\%))$.

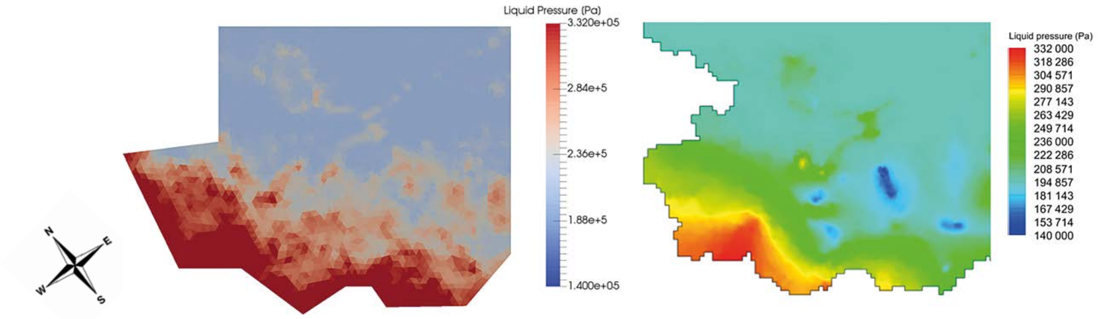
N
E
W
S
Liquid Pressure (Pa)
3.320e+05
2.84e+5
2.36e+5
1.88e+5
1.400e+05
Liquid pressure (Pa)
332 000
318 286
304 571
290 857
277 143
263 429
249 714
236 000
222 286
208 571
194 857
181 143
167 429
153 714
140 000

Figure 2-12. *Qualitative comparison of pressures at the top layer (t = 3500 AD).*

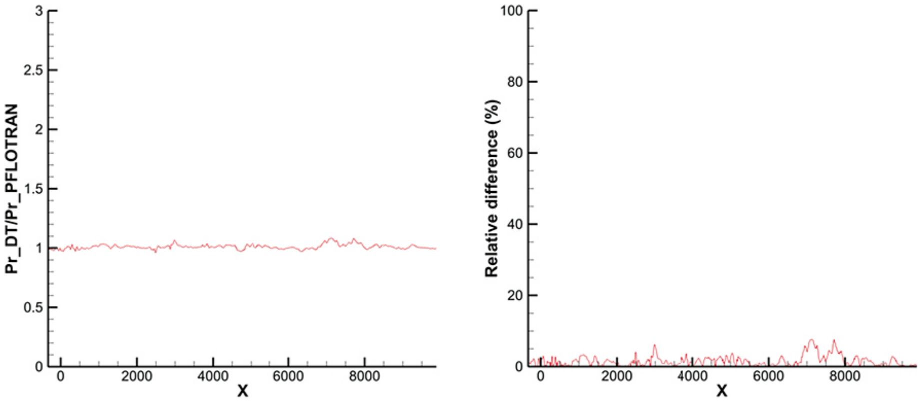

Figure 2-13. *Quantitative comparison of pressures over the line: x ∈ [−328, 9880], y = 8640, z = −20 m at t = 3500 AD.*

As it can be seen in the plots (Figures 2-11 and 2-13), the interpolation error is low, which validates the approach as a good way to approximate the DT pressure boundary conditions into PFLOTRAN.

Regarding to the initial conditions used in the model, a hydrostatic pressure field has been applied:

$$p(z) = p_0 - \rho g z \tag{3-1}$$

Where p(z) is the pressure at height z, p_0 is the reference pressure, ρ the water density, g the acceleration of gravity and z the height. For convergence reasons, this pressure field is built externally to exactly fit the boundary conditions of the model and it is imported in PFLOTRAN using an HDF5 file. However, before generating any pressure fields, the following two points need to be considered:

1. PFLOTRAN uses total pressure in its calculations, while DT is based on residual pressure.
2. The reference pressure (p_0) to calculate the unsaturated zone is $p_0^{DT} = 0$ in DT and $p_0^{PFLOTRAN} = 101325$ Pa in PFLOTRAN.

Related to the first point, the hydrostatic component needs to be added to the DT pressure field. Thus, following the criteria shown in Figure 2-14,

$$p_i^{PFLOTRAN} = p_i^{DT} - \rho_w g(z_i - z_{i(top)}) \tag{3-2}$$

where $p_i^{PFLOTRAN}$ is the total PFLOTRAN pressure, p_i^{DT} states for the DT pressure, ρ_w is the water density, g is the gravity, z_i is the z-component of the mesh element n ($i = n$) and $z_{i(top)}$ is the topography elevation that corresponds to the *n* mesh element. The topography height ($z_{i(top)}$) is the highest z value for a given point in the X-Y plane.

The reference pressure must be taken into account when unsaturated flow is considered. The DT model uses negative pressure values to describe the unsaturated zones of the mode ($p_0^{DT} = 0$)). In PFLOTRAN, the reference pressure at which the model begins to get unsaturated is at the atmospheric pressure (101 325 Pa) instead of 0:

$$\text{Darcy Tools}\begin{cases}\text{saturated} & \text{if} \quad p_i^{DT} > 0\\ \text{unsaturated} & \text{if} \quad p_i^{DT} < 0\end{cases}$$

$$\text{PFLOTRAN}\begin{cases}\text{saturated} & \text{if} \quad p_i^{PFLOTRAN} > p_0^{PFLOTRAN}\\ \text{unsaturated} & \text{if} \quad p_i^{PFLOTRAN} < p_0^{PFLOTRAN}\end{cases}$$

where $p_0^{PFLOTRAN} = 101325$ Pa.

By considering the aforementioned points, the DT pressure must be modified according to Equation (3-3) before importing it into PFLOTRAN.

$$p_i^{PFLOTRAN} = p_i^{DT} + p_0^{PFLOTRAN} - \rho_w g(z_i - z_{i(top)}) \tag{3-3}$$

Once the data corresponding to the three restart time steps is interpolated, a unique HDF5 file is built for both the top and the bottom layers. This file allows PFLOTRAN to automatically update the pressure field at the times indicated in Figure 2-15. The names and contents of the associated files are listed in Appendix (Table A-1).

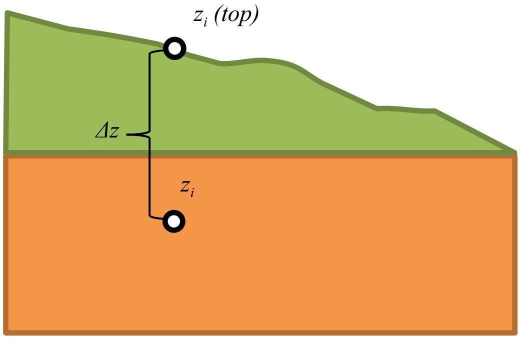

Figure 2-14. *Diagram showing the i-th mesh element height (z_i) and the associated topography elevation ($z_{i(top)}$).*

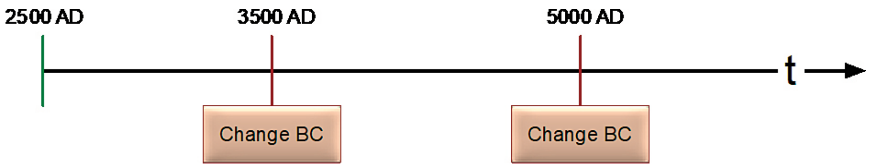

Figure 2-15. *Diagram showing the times when the pressure fields are updated.*

2.3.3 Initial and boundary conditions for reactive transport

One of the most important sources of uncertainty in the context of geochemical modelling in crystalline rocks is the chemical composition of the fracture filling and its distribution in the fractures. In addition, and despite the heterogeneous distribution observed on site, most of geochemical models assume a homogeneous mineral distribution in the fracture fillings in contact with groundwaters. Thus, the presence/absence of minerals is usually assessed by means of sensitivity analysis varying the minerals involved in the reactions and their characteristics (amounts, surface areas, cation exchange capacity). The most reactive minerals dissolve/precipitate to instantaneously attain equilibrium conditions and the less reactive ones will react kinetically.

The chemical calculations implemented in the 3D models are based on the same set of geochemical constraints defined in Román-Ross et al. (2014). Groundwater interaction with the fracture filling minerals is defined by imposing equilibrium conditions with calcite/ hematite for the Base Case and calcite/FeS(am) for the Variant case. These two cases were selected to cover uncertainties linked to mineral phases controlling redox conditions. The redox conditions vary considerably with depth and generally appear to be dominated by reactions involving various iron and sulphur species. Data analyses and modelling of the redox system indicate that reducing conditions currently prevail at depths greater than about 20 m (Crawford 2008). Fe-oxyhydroxides, mainly hematite, are present in hydraulically conductive fractures and fracture zones. This suggests oxidised conditions have prevailed in some period of time in parts of the fracture system (Sandström et al. 2014). No occurrences of sulphides have been recorded in hydraulically conductive fractures in the upper 30 m of the bedrock at SFR, probably having been dissolved during events of intrusion of oxygenated fluids. However, no significant oxidation and/or dissolution of sulphide due to inflow of oxidized waters have been identified in the drill cores below 30 m (Nilsson et al. 2011). Despite the uncertainty of the measured data, the dissolved sulphide concentrations at shallow to intermediate depths are low, and the dissolved sulphide concentrations increase, which is consistent with the active precipitation of ironmonosulphides (Crawford 2008). Calculations performed with the base and the variant case in this study consider these particularities and assess redox conditions depending on mineral phase involved on redox control.

In our models, the number of processes considered for describing groundwater-fracture filling interactions was reduced (e.g. cation exchange reactions were not implemented) to save CPU time and optimise calculations. Clay minerals could have an active role in the final composition of groundwaters. However, a comparison between the computed results with FASTREACT (Román-Ross et al. 2014) with the range of concentrations reported by Auqué et al. (2013), seems to indicate that clays with high CEC are not available in this SFR geochemical system.

Figure 2-16 displays a sketch of the initial conditions prescribed at 2500 AD, 3500 AD and 5000 AD. The initial concentrations assumed for the boundary and fracture waters are shown in Table 2-2. Solute transport occurs by advection along the fracture and by diffusion in the rock matrix pores. The recharge flow paths were taken from a DarcyTools model that simulates temperate hydrogeological conditions (see Section 2.2 and Appendix). SFR is covered today by the Baltic Sea, however, due to the ongoing shoreline displacement, the boundary conditions (*i.e.* fluxes of infiltrating waters) will evolve in time and the influence of meteoric water is expected to become more important.

The chemical composition of the boundary and fracture waters used in calculations for the different climate domains are compiled in Table 2-2. Boundary meteoric water corresponds to a real sample of meteoric water (HBHO2, 1931) in Salas et al. (2010, p 165). Due to the lack of reported concentrations of Al and Fe, both elemental contents have been taken from the "Altered Meteoric Water" defined by Salas et al. (2010, p 37). Fracture water (i.e. initial water present in the fracture) is assumed to have the chemical composition defined by Auqué et al. (2013, Table 5-2) (i.e. penetrating brackish water). Aluminium concentration is assumed to be in equilibrium with kaolinite.

The conceptualization of rock matrix diffusion processes is developed in the next chapter.

Table 2-2. Chemical composition of boundary and fracture waters.

Parameter	Boundary meteoric water	Fracture water
pH	7	7.3
pe	0.55	−3.81
Concentration (M)		
Al	7.72×10^{-8}	6.38×10^{-8}
HCO_3^-	1.03×10^{-3}	1.28×10^{-3}
Ca	3.85×10^{-4}	1.50×10^{-2}
Cl	1.41×10^{-4}	9.87×10^{-2}
Fe	1.79×10^{-6}	1.11×10^{-8}
K	5.88×10^{-5}	5.13×10^{-4}
Mg	7.82×10^{-5}	6.17×10^{-3}
Na	5.00×10^{-4}	6.52×10^{-2}
SO_4^{2-}	1.38×10^{-4}	3.65×10^{-3}
$SiO_{2(aq)}$	1.21×10^{-4}	1.83×10^{-4}

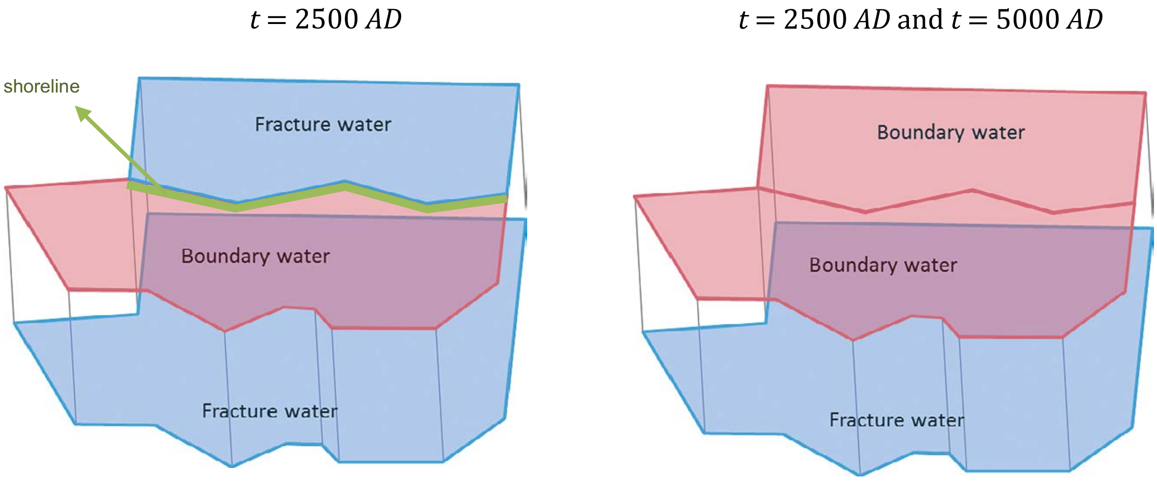

$t = 2500\ AD$

$t = 2500\ AD$ and $t = 5000\ AD$

shoreline
Fracture water
Boundary water
Fracture water
Boundary water
Boundary water
Fracture water

Figure 2-16. Summary of the transport boundary conditions prescribed in the model.

3 Rock matrix diffusion

Besides simulating flow and reactive transport processes in the upscaled Equivalent Continuous Porous Medium (ECPM), the influence of the matrix and its related geochemical reactions must be accounted for. This process describes diffusion from/to fracture water into the rock matrix and impact on the final composition of fracture waters depending on several parameters as rock composition, matrix porosity (connected porosity) and the extend of altered zone around the fracture.

In this model, we used the Multiple Continuum Approach derived by Lichtner (2000). This approach is already included into PFLOTRAN but has never been tested comprehensively. Thus, several verification exercises were conducted for cross-checking the robustness of this method to simulate matrix diffusion (Section 3.2).

Multicontinuum models attempt to represent the fractured porous media as two interacting continua: one corresponding to the fracture network and the other one to the matrix. Thus, rock matrix interaction with the fracture system can be quantified. These models are particularly appealing due to their numerical efficiency. A single fracture-matrix system was simulated using the following approaches:

- 1D model (No rock matrix)
- 1D multicontinuum model
- 2D model (explicit model)
- Analytic solution (Tang et al. 1981)

The objective of this benchmark is to validate the multicontinuum approach by comparing the 1D multicontinuum model with an equivalent 2D model (*i.e.* which explicitly model the fracture-matrix system) and an analytical solution. The 1D model without multicontinuum and reactive matrix is used as a synthetic reference.

3.1 Model description

3.1.1 1D model

A sketch of the 1D model is shown in Figure 3-1. A constant flux (v_{flux} = 0.066 m/day) is applied to the left boundary of the fracture and a Dirichlet boundary condition (i.e. prescribed pressure) is set at the right boundary. A conservative tracer is injected at the inlet and its breakthrough curve is observed at the outlet point.

The flow and transport boundary conditions remain unchanged over time. However, in the multicontinuum approach, an extra dimension is added to every spatial node to simulate the rock matrix (i.e. a secondary continuum). The implementation of the secondary continuum in PFLOTRAN, requires to calculate some geometrical properties that are based on the 2D fracture-matrix system.

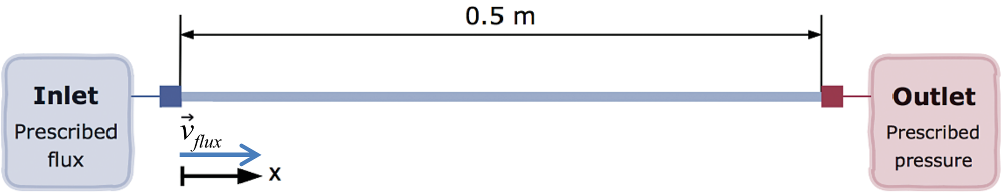

Figure 3-1. *Model sketch of the 1D model.*

As the model shows spatial symmetry over the z-axis (Figure 3-2), only one half of the model needs to be considered. Assuming arbitrarily the half-fracture aperture ($\delta = 1.58 \times 10^{-3}$ m) and the half-fracture spacing ($L = 9.8 \times 10^{-2}$ m) the fracture volume fraction and the fracture-matrix specific surface (i.e. the ratio between the interfacial area and the total volume) can be calculated as follows:

Fracture volume fraction: $\epsilon_f = \frac{\delta}{\delta + L} = 0.0159$ (3-4)

Fracture-matrix specific surface: $A_{fm} = \frac{1}{L}(1 - \epsilon_f) = \frac{1}{\delta + L} = 10.04 \text{m}^{-1}$ (3-5)

Regarding the other related parameters, tortuosity is set to $\tau = 0.1$, and the diffusion coefficient in free water is 1×10^{-9} m²/s which gives a pore diffusion coefficient of $D_p = D_0\tau = 1 \times 10^{-10}$ m²/s. The porosity of the matrix is set arbitrarily to $\phi_m = 0.01$. Note that the term "tortuosity" is here used in the same sense of de Marsily (1986), i.e. as the ratio between pore diffusivity and molecular diffusion in free water.

The conceptual model behind this secondary continuum approach is denoted as Slab model inside PFLOTRAN.

3.1.2 2D model

In the 2D model (Figure 3-3), the fracture-matrix system is modelled explicitly, using the same parameters as in the multicontinuum model. The 2D model has been meshed in a structured way using 250 cells on the y-direction (i.e. along the fracture) and 750 cells on the z-direction. This makes a total of 187 500 mesh elements.

To improve the numerical robustness of the model, the discretization of the mesh varies depending on how close it is from the fracture-matrix interface. Thus, the mesh elements that are close to the fracture-matrix interface are finer than the ones that are further away (Figure 3-3).

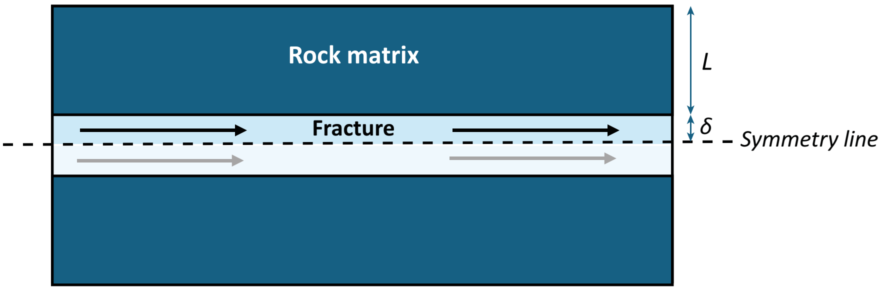

Figure 3-2. *Sketch representing the 1D multicontinuum model.*

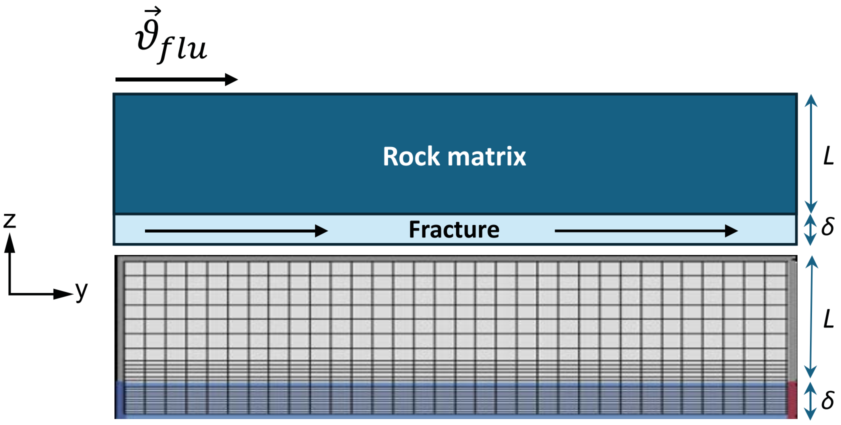

Figure 3-3. *Sketch of the 2D model.*

This model is a key tool for validating the 1D multicontinuum approach since it simulates explicitly the fracture-matrix system and it can be taken as the reference simulation if an analytical solution is not available.

3.1.3 Analytical resolution

The analytical solution used in this verification exercise (Tang et al. 1981) simplifies the 2D fracture-matrix diffusion problem as two coupled, one-dimensional partial differential equations: one for the fracture and one for the porous matrix in a direction perpendicular to the fracture.

The same assumptions as in Tang et al. (1981) are made relating to the geometry and hydraulic properties of the system:

1. "The aperture of the fracture is much smaller than its length"
2. "Transverse diffusion and dispersion within the fracture assure complete mixing across the fracture aperture at all times."
3. "The permeability of the porous matrix is very low and transport in the matrix will be mainly by molecular diffusion."
4. "Transport along the fracture is much faster than transport within the matrix."

Since the multicontinuum approach presented here is in agreement with the above assumptions, this analytical solution should be a good reference to validate and compare it with.

The analytical solution solves the coupled fracture-matrix differential equations using the Laplace transform. Two partial differential equations (PDE) are used to describe the transport phenomena in both the fracture and the matrix. The PDE for the matrix domains is shown in Equation 3-6.

$$\frac{\partial c'}{\partial t}-\frac{D^{eff}}{R'}\frac{\partial^2 c'}{\partial x^2}+\lambda c'=0 \qquad (3\text{-}6)$$

where c' is the concentration of solute in the matrix domain, x is the coordinate along the matrix domain, λ is the decay constant, $D^{eff} = \tau D^*$ is the effective diffusion coefficient (i.e, the molecular diffusion coefficient, D^0, times de matrix tortuosity, τ) and R' is the matrix retardation coefficient, which is defined as,

$$R'=1+\frac{\rho_b}{\theta}K_m \qquad (3\text{-}7)$$

being ρ_b the bulk density of the matrix, θ the matrix porosity and K_m the matrix distribution coefficient.

The PDE for the fracture domain is described in Equation 3-8

$$\frac{\partial c}{\partial t}+\frac{v}{R}\frac{\partial c}{\partial z}-\frac{D}{R}\frac{\partial^2 c}{\partial z^2}+\lambda c-\frac{\phi D^{eff}}{bR}\frac{\partial c'}{\partial x}\bigg|_{x=b}=0 \qquad (3\text{-}8)$$

where c is the concentration of solute in the fracture domain, v is the groundwater velocity in the fracture, z is the coordinate along the fracture axis, b is the half-fracture aperture and corresponds to the location of the fracture-matrix interface, and R is the retardation factor defined at Equation 3-9.

$$R=1+\frac{K_f}{b} \qquad (3\text{-}9)$$

being K_f the distribution coefficient, defined by Freeze and Cherry (1979) as the mass of solute adsorbed per unit area of surface divided by the concentration of solute in solution. The factor $\frac{\phi D^{eff}}{bR}\frac{\partial c'}{\partial x}\Big|_{x=b}$ represents the diffusive flux that comes from the matrix into the fracture zone.

The PDE is then transformed to the Laplace space where it reduces into an ordinary differential equation. Equation 3-10 shows the solution in the Laplace space:

$$\hat{c}(P)=\frac{c_0}{P\text{-}\lambda}\exp \nu z \exp\left[\text{-}\nu z\left\{1+\beta^2\left[\frac{P^{1/2}}{A}+P\right]\right\}\right] \qquad (3\text{-}10)$$

Here, P is the Laplace variable, C_0 is the initial concentration, λ stands for the decay constant (since the solution is also valid for decaying radionuclides), $\nu = v/2D$, where v is the groundwater velocity in the fracture, z is the coordinate along the fracture axis, $\beta^2 = 4RD/v^2$ and A is defined as

$$A = \frac{bR}{\left(\theta R' D^{eff}\right)^{1/2}} \tag{3-11}$$

where b is the half-fracture aperture.

Finally, the inverse of the Laplace transform is numerically computed using de Hoog algorithm (see de Hoog et al. 1982) (Hollenbeck 1998). Octave (Eaton et al. 2014), a programming language that is focused on mathematical modelling, has been used to build the script which inverses the Laplace transform and gets the solution in the time domain.

3.2 Verification tests

The three models mentioned in Chapter 3 have been run with a tracer using PFLOTRAN for a simulation time of 20 days. A fine temporal discretization as well as strict tolerances have been used to minimise numerical dispersion. The breakthrough curves obtained with the different models are shown in Figure 3-4.

In the 1D model (without matrix diffusion), an earlier first-time arrival is observed compared to the other models. Moreover, the breakthrough curve reaches a plateau value of 1.0 after 10 days (*i.e.* injection concentration). The solution of the 1D multicontinuum model well agrees with the explicit 2D fracture-matrix model as well as with the analytical solution (Figure 3-4). A retardation effect is clearly observed as result of diffusion in the rock matrix. The slight differences observed between the 1D (with multicontinnum) and the 2D models are due to the higher numerical dispersion shown by the 2D model.

In conclusion, this first verification test is considered successful. However, to fully validate the proposed approach, further verification cases are required. Next section focuses on the simulation and verification of a reactive matrix system.

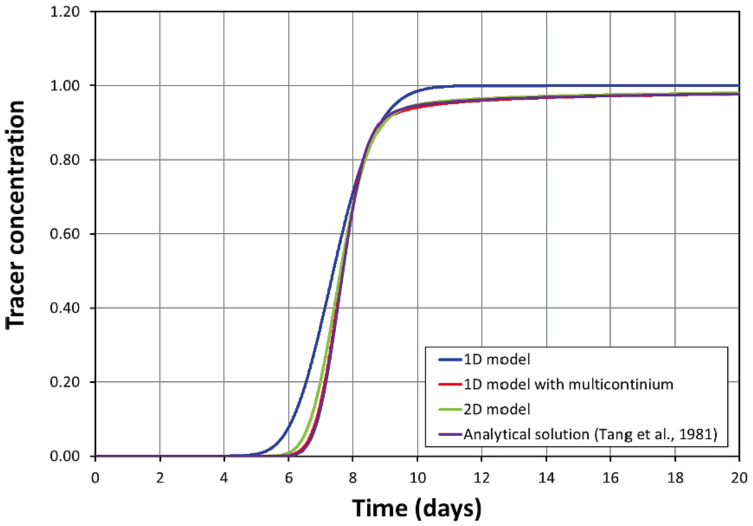

Figure 3-4. *Comparison of breakthrough curves of a tracer for the different numerical approaches. The purple line of the analytical solution is partly obscured by the red line (early times), but also the green line (later times).*

3.3 Matrix diffusion verification under reactive conditions

A calcite dissolution model under equilibrium conditions (Equation 3-10) has been considered as a benchmark exercise to test matrix diffusion under reactive conditions. Figure 3-5 summarizes the model set-up. The concentrations of the chemical species prescribed in the inlet and the initial waters are listed in Table 3-1. Similar to the non-reactive case, inlet water is injected through the inlet boundary (y = 0). All the parameters and input specifications of this test are taken from the 'Calcite Dissolution' regression test of PFLOTRAN (Lichtner et al. 2015, Iraola et al. 2019). Initial water is slightly basic and is in equilibrium with calcite while the inlet water is slightly acidic. Thus, it is expected that the progressive penetration of the boundary water deep into the matrix will lead to the dissolution of calcite, which in turn will buffer the acidic conditions.

$$CaCO_3 \rightleftarrows Ca^{2+} + CO_3^{2-} \tag{3-12}$$

Table 3-1. Primary species concentrations in the reference waters.

	Initial water	Inlet water
pH	8	5
HCO_3^-	1.0×10^{-3} M	1.735×10^{-3} M
Ca^{2+}	1.718×10^{-4} M	5.0×10^{-4} M

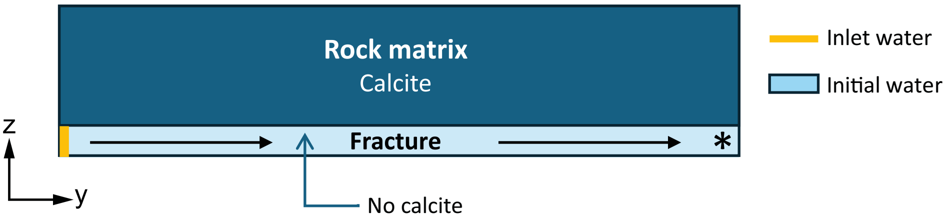

Figure 3-5. *Model set-up of the calcite dissolution model. The * represents the observation point.*

The model has been run varying the number of cells in the secondary continuum. The starting number of cells in the secondary continuum is 20 cells. Since the comparison with the 2D model was not good, new cases with increasing number of cells in the secondary continuum have been considered. The desired match with the 2D model has been obtained using 500 cells in the secondary continuum. Groundwater-rock matrix interactions have been evaluated by mean of breakthrough curves (pH and Ca concentrations) obtained in the outlet point (Figure 3-6).

The results show a strong dependence on the number of secondary continuum cells resulting on poor performance when the number of cells is less than 500. Considering that the number of secondary continuum cells needed to reproduce the 2D model (Equation 3-13) is of around 500, the total number of mesh elements would also increase by a factor of 500 (i.e. the Degrees Of Freedom (DOF) of the model would increase by the same factor). Thus, the amount of computational resources needed to build a functional 3D model would be too high.

$$N_{model} = N_{sec} \cdot N_{mesh} \tag{3-13}$$

Here, N_{model} represents the total number of elements of the coupled (primary and secondary continuum) model, N_{sec} is the number of elements of the secondary continuum block and N_{mesh} is the number of elements of the primary continuum.

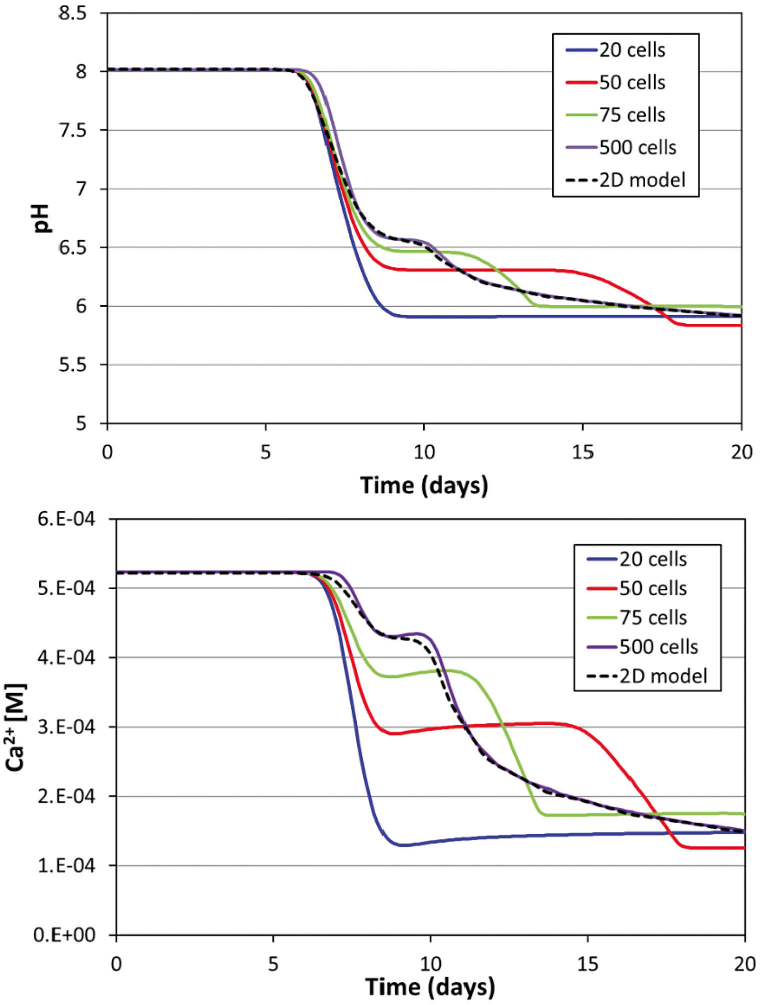

Figure 3-6. *pH and Ca^{2+} concentration evolution over time (measured at the observation point) for the 1D multicontinuum model (colours correspond to different values of the secondary continuum cells) and the 2D fracture-matrix model. Diagrams modified from Iraola et al. (2019).*

However, PFLOTRAN offers more than one way to build the secondary continuum. In particular, there is an implementation called ‘Nested Cubes’ that allows building a secondary continuum that follows a logarithmic grid distribution. The following section test the viability of such approach to scale and build a fully functional 3D model.

3.3.1 Nested cubes approach

The nested cubes approach considers a cubical fracture-matrix system. Here, matrix boxes are surrounded by a fracture coating in all their faces. Figure 3-7 shows a sketch of the nested cubes approximation.

The parameters used in the previous approach (i.e. the Slab approach) can be adapted straightforwardly into the Nested cubes approach. The equivalence between them is displayed in Table 3-2. More details can be found in Iraola et al. (2019).

Table 3-2. Equivalence between the Nested cubes and the Slab approaches.

Slab	Nested cubes
Half-fracture aperture: δ	Fracture-spacing: $l_f = L + 2\delta$
Matrix size: L	Matrix-spacing: $l_m = L$
Fracture volume: $V_f = \delta ab$	Fracture volume: $V_f = l_f^3 - l_m^3 = (L+2\delta)^3 - L^3$
Total volume: $V_{tot} = (\delta + L)ab$	Total volume: $V_{tot} = l_f^3 = (L+2\delta)^3$
Fracture volume fraction: $\epsilon_f = \frac{\delta}{\delta + L}$	Fracture volume fraction: $\epsilon_f = 1 - \frac{l_m^3}{l_f^3} = 1 - \frac{L^3}{(L+2\delta)^3}$

To test the new approach, the calcite dissolution example has been modelled again applying a logarithmic grid distribution in the secondary continuum. This can be done automatically in PFLOTRAN using the LOG_GRID_SPACING option and tuning a weight parameter α. The weight parameter allows the grid to be more refined in the first cells of the secondary continuum (i.e. close to the fracture-matrix interface), and thereby the results will be are considerably improved.

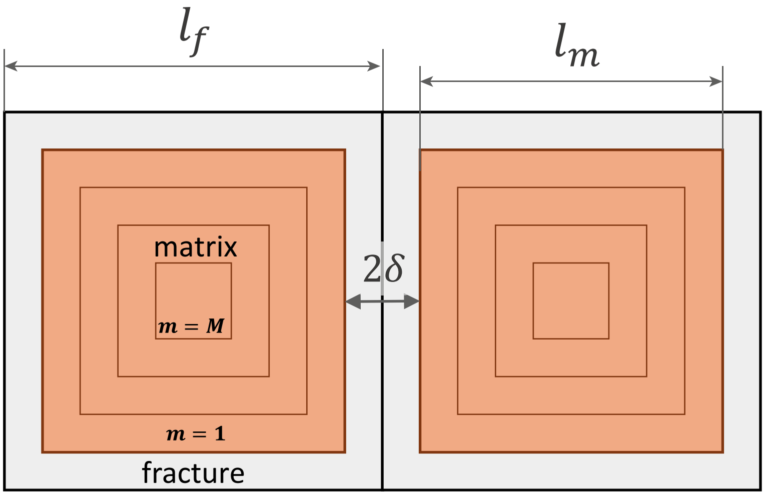

Figure 3-7. Sketch of the Nested cubes multicontinuum approach.

Figure 3-8 shows the evolution of pH and Ca^{2+} in an elapsed time of 20 days for different values of the weight parameter α. All the simulations were run with 20 cells in the secondary continuum. As in the previous section, an equivalent 2D model is used as a reference case (i.e. because there is not an analytical solution to the calcite dissolution problem).

The results show that the breakthrough curves of the 1D multicontinuum model converge to the reference 2D model when small values of the parameter α are used ((Figure 3-8). It is worth mentioning that only 20 secondary continuum cells were used to run the models resulting in 20 times bigger models. This computational size is feasible to scale into a full 3D model. Thus, it can be concluded that, after calibrating the weight parameter to the current chemical system, the multicontinuum approach is a valid approach to simulate fracture-matrix diffusion under reactive conditions.

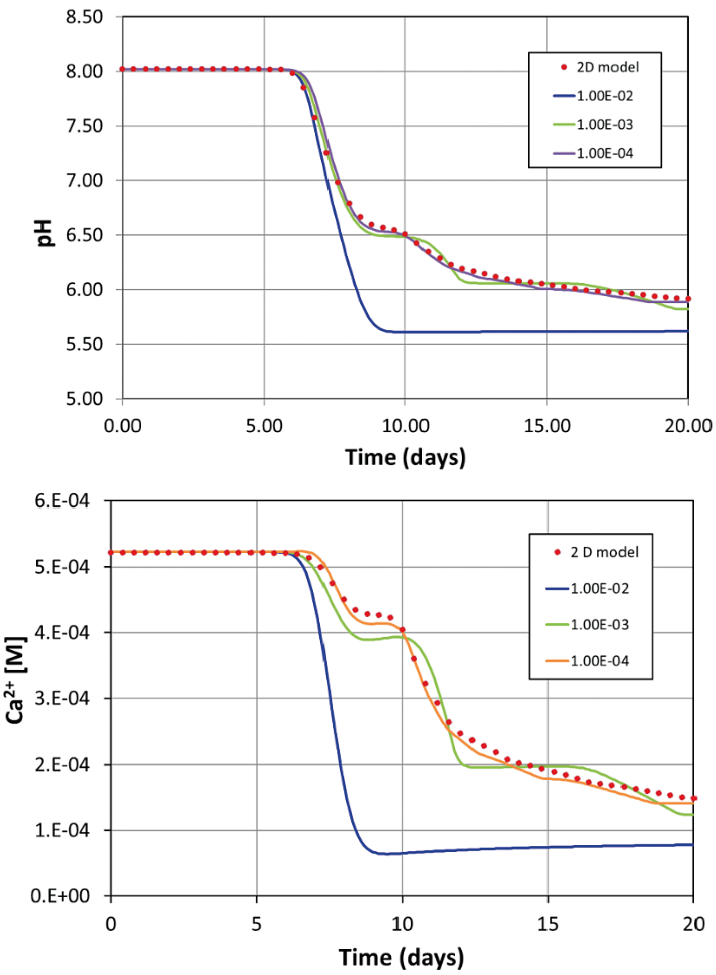

Figure 3-8. *Comparison of pH and Ca^{2+} concentrations computed in the observation point between the 2D model and the 1D multicontinuum model for different values of the logarithmic weight parameter α. Diagrams modified from Iraola et al. (2019).*

3.4 Verification example applied to the SFR repository

As stated in the previous section, the parameters used for implementing the secondary continuum need to be adjusted to the chemical system applied in this study. This section includes the benchmark test adapted for calibrating the model´s parameters.

3.4.1 Numerical model

The variant case geochemical model (Section 2.3.3) was used for the last verifications of the multi-continuum method. In this case, we implemented the numerical formulation used in the previous case (Section 3.3.1) updating matrix conceptualization to the chemical reactions that will be included in the 3D model. Figure 3-9 schematically shows the selected parameters.

Rock matrix parameterization is an important source of uncertainties in geochemical models. In natural environments, the rock matrix could extend between a few millimetres to several meters in highly fractured zones. We have implemented a 3-meter reactive zone to estimate maximal effects due to rock matrix- groundwaters interactions. In terms of composition, this alteration zone adjacent to fractures, usually presents a complete or partial alteration of plagioclase and K-feldspar, biotite and iron minerals. For the sake of simplification, we selected biotite ($K\,Mg_{1.5}Fe_{1.5}\,AlSi_3O_{10}(OH)_2$) as the sole mineral potentially able to kinetically dissolve in the rock matrix. Clearly, this is a first simplified assumption but needed to test the reliability and robustness of the model. It is important to mention that silicate mineral kinetic dissolution is a process with implications in pH buffering mechanisms in groundwaters. Therefore, water chemistry will be modified by chemical reactions that consume protons and release cations and silica.

One of the most pertaining parameters related to mineral availability in the rock matrix is matrix porosity. Sidborn et al. (2010) reported a wide range for median value of connected porosity in altered metamorphic granite to granodiorite rocks (0.75 vol%, range 0.50 – 0.93 %) and unaltered rocks (0.42 vol%, range 0.28 – 0.66 %). We have implemented in our calculations the value suggested for use in the Data report for SR-Site (0.18 vol%) (SKB 2010, TR-10-52) and fully agrees with the range of surface area values reported in Trinchero et al. (2017).

The rock matrix porosity also define the available mineral surface areas involved in the kinetic dissolution of biotite. The models were run considering 1 105 m^2/m^3, ($A_{biotite}$ in Figure 3-9). This value is one order of magnitude lower than the lower values reported by Sidborn et al. (2010) and fully agrees with the range of surface area values reported in Trinchero et al. (2017). A first test confirmed that by using 11 050 m^2/m^3, inconsistent results are obtained due to the high reactivity of the altered zone considered in the model. Parameterization of rock matrix is a very challenging task because of upscaling of laboratory data to a reactive model assuming, for instance, a homogeneous distribution of biotite in a large domain. In addition, matrix porosity is other source of uncertainty. Calculation of surface area values requires a value of interconnected porosity, a parameter difficult to obtain.

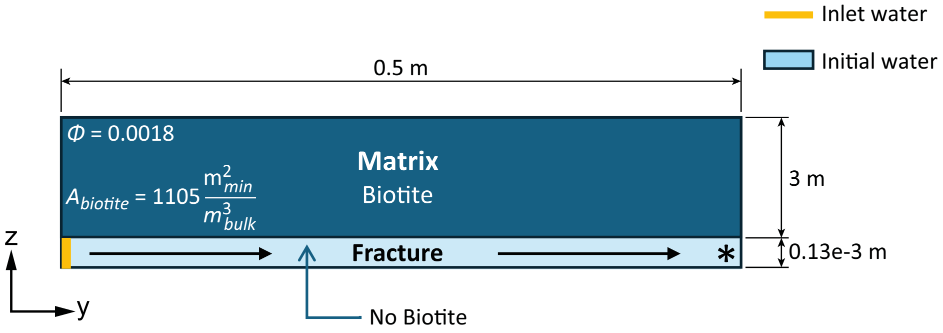

Figure 3-9. *Parameters of the rock matrix used in the model. The * represents the observation point. The fracture aperture value was taken from Sidborn et al. (2014).*

Kinetic dissolution of biotite was implemented according to the reaction described in Equation 3-14 and the kinetic dissolution rate reported in Palandri and Kharaka (2004). The chemical composition of initial reference waters is listed in Table 2-2.

$$\mathrm{K\,Mg_{1.5}Fe_{1.5}\,AlSi_3O_{10}(OH)_2 + 10H^+ + Al^{3+} + K^+ + 1.5\,Fe^{2+} + 1.5\,Mg^{2+} + 3\,SiO_2(aq) + 6\,H_2O} \quad (3\text{-}14)$$

The simulations have been run for 30 days for both the 1D multicontinuum and the 2D fracture-matrix cases. Figure 3-10, 3-11 and 3-12 show the breakthrough curves computed for some key parameters at the observation point (Figure 3-9). As a consequence of their mutual interdependence, redox conditions are affected by the increase in pH and a decrease in the pe values is observed when pH values rise up to values around 8 (Figure 3-10).

The results indicate that the multicontinuum approach is a validated tool to simulate fracture-matrix diffusion under reactive matrix conditions. A good agreement is observed between the 1D model run with multicontinuum and the 2D model. The release of elements provided by biotite are clearly identified in the fracture water (Figure 3-11 and Figure 3-12). As Na is not included in biotite composition, it can be assumed as a tracer. Figure 3-12 display a very good match among all the computed cases. In the case of Al concentrations, the differences observed between the 2D model and 1D model with multicontinuum can be attributed to scale effects magnified by the low initial Al concentrations (Figure 3-11). Dissolved silica inputs from the matrix to the fracture domain is evidenced by the higher concentrations computed with the multicontinuum approach.

Fe and Mg are provided in equivalent molar concentrations by biotite to the pore-matrix water and, in turn, *via* diffusion to the fracture groundwater. Magnesium concentrations increase with time as any process attenuate its concentrations in the fracture domain (Figure 3-12). The rock matrix also behaves as a source of Fe^{2+} but, due to precipitation of FeS(am) prescribed in the fracture domain, the concentrations observed at the observation point are lower than those computed for the non-reactive model (without multicontinuum).

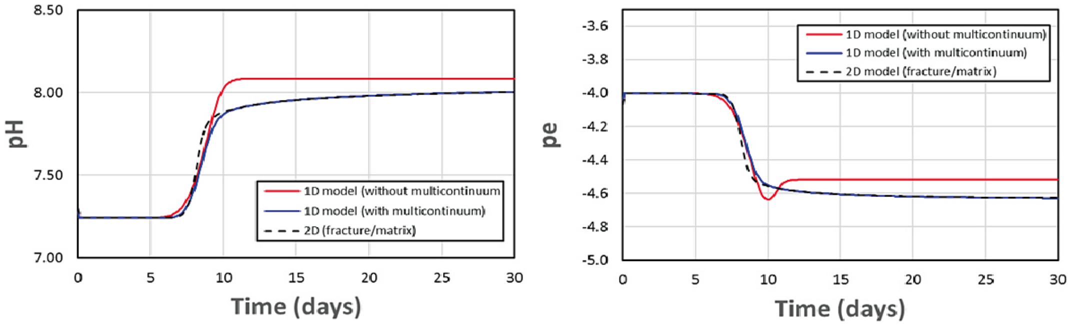

***Figure 3-10.** pH and pe breakthrough curves at the observation point computed for the 2D model and the 1D multicontinuum/no-multicontinuum models.*

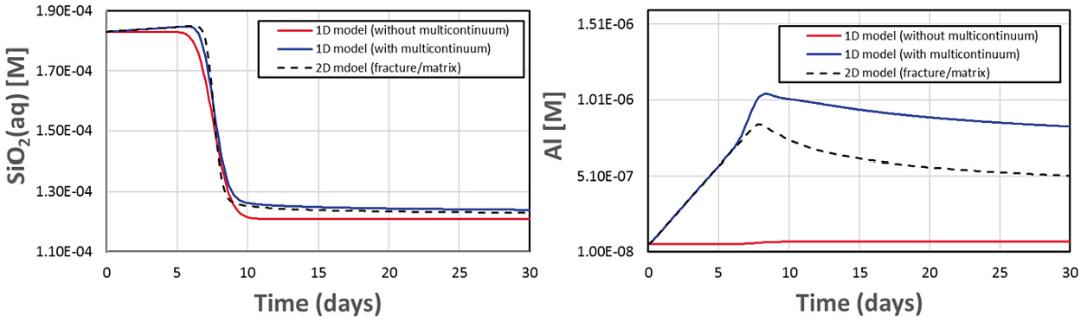

***Figure 3-11.** SiO_2(am) and Al concentrations computed at the observation point for the 2D model and the 1D multicontinuum/no-multicontinuum models.*

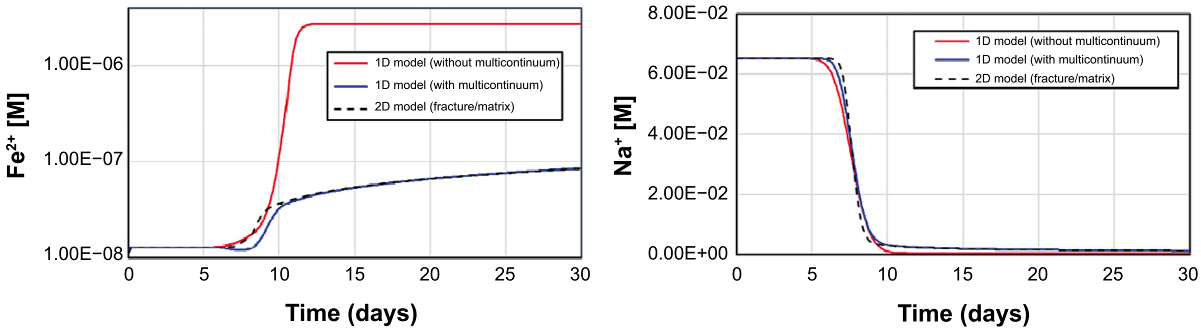

Figure 3-12. *Fe^{2+} and Na^{+} concentrations computed at the observation point for the 2D model and the 1D multicontinuum/no-multicontinuum models.*

3.5 Implementation of the multicontinuum approach into the 3D model

Before implementing the multicontinuum approach into the 3D model, two issues need to be carefully evaluated. The first one is related to the computational size of the model. The multicontinuum approach adds a forth mathematical dimension to the model, for each spatial node there is an extra dimension that simulates the matrix (*i.e.* the secondary continuum). This increases the number of degrees of freedom of the model significantly (see Equation 3-13).

The standard workstations used to run the previous models did not have enough computational power to simulate the full multicontinuum model. Thus, these simulations have been run on the supercomputer JUQUEEN of the Jülich Supercomputing Centre.

3.5.1 Flow velocity issue

When the multicontinuum approach is considered, the current PFLOTRAN version computes the flow velocity in a different way than usual:

$$v_{multi} = \frac{v_0}{\epsilon_f} \tag{3-15}$$

There, v_{multi} stands for the multicontinuum velocity, v_0 is the Darcy's velocity and ϵ_f is the fracture volume fraction. This implies that the computed velocity for the multicontinum case is higher than the usual velocity (since $0 < \epsilon_f < 1$), and inconsistent results could be computed.

In the 1D benchmarks, this issue has been easily overcome by changing the initial Darcy velocity according to Equation 3-13. However, in the 3D model, this cannot be done straightforwardly. The following workaround has been implemented to solve the issue.

On the one hand, PFLOTRAN does not allow changing the velocity field node-per-node, so the velocity cannot be rescaled as in the 1D case. On the other hand, changing the dimensions of the model (i.e. making them bigger), would imply a complete re-modelling of the geometry and mesh. Thus, the most reasonable workaround to deal with the higher velocities is to rescale time. This can be implemented easily by multiplying all the times present in the model by the fracture volume fraction:

$$t_{multi} = t_0 \cdot \epsilon_f \tag{3-16}$$

where t_{multi} is the rescaled time, t_0 the no-multicontinuum time and ϵ_f stands for the fracture volume fraction. A couple of tests have been done to validate this approach. The outcomes of these tests give give a fracture volume fraction of $\epsilon_f = 2.167 \times 10^{-4}$ for the geometrical model parameters (*i.e.* $\delta = 0.13 \times 10^{-3}$ and L = 3 m) considered in the simulation.Table 3-3 shows both the original times and the rescaled ones.

Table 3-3. Original and rescaled times for the multicontinuum approach.

	No-multicontinuum	Multicontinuum
Starting time	0 y	0 y
1st update	1 000 y	0.25995 y
2nd update	2 500 y	0.649875 y
Final time	2 500 y	0.909825 y
Timestep	25 y	0.00649875 y

3.5.2 Unsaturated flow

When unsaturated flow and the multicontinuum approach are running together, the current PFLOTRAN version fails to properly calculate the concentrations of the chemical species (i.e. it does not conserve mass). To fix the issue, the pressure field used in the multicontinuum model has been uplifted until a fully saturated model is obtained. This has been done adding the reference pressure to each node of the PFLOTRAN pressure (Equation 3-17)

$$p^i_{multi} = p^i_{PF} + p_{ref} \tag{3-17}$$

Here, p^i_{PF} is the pressure at the *i*-th node of the no-multicontinuum model, p^i_{multi} the calculated new pressure and p_{ref} = 101325 Pa.

The data sources are listed in Appendix (Table A-1). In addition, in Table A-2, the complete list of simulations performed are referenced with the names of the inputs/outputs delivered to SKB.

4 3D model with reactive matrix

This section provides illustration of the 3D reactive transport models implemented for geosphere surrounding the SFR repositories. In Chapter 3, the multicontinuum matrix diffusion approach has been tested in a 1D reactive transport model and the results have been adequately validated. In order to apply this concept to a large-scale model, two different geochemical models were run with the hydrogeological model previously described in Chapter 2. The reactive transport calculations denoted as the Base Case, consider hematite under the assumption of local equilibrium with the fracture filling minerals. An alternative geochemical case, denoted as the Variant Case, has been defined imposing chemical equilibrium with respect to FeS(am) instead of hematite. The reason behind this choice is justified by the uncertainties in the composition and distribution of fracture fillings minerals (Román-Ross et al. 2014). In both cases, we considered a reactive rock matrix where biotite is kinetically dissolved interacting with fracture groundwater through diffusion processes. The rock matrix parametrization shown in Section 3.4.1 (Figure 3-9) was implemented in these 3D models. Additional runs without a reactive matrix were computed and used as reference cases for assessing the impact of matrix diffusion processes on the final composition of fracture groundwaters.

The numerical simulations were run for an elapsed time of 3 500 years (from 2500 AD to 6000 AD) during the temperate period. During this period, a displacement of the shoreline is predicted as a consequence of isostatic uplift. Thus, the displacement of the Baltic shoreline will influence the hydrology of the site. As shown in Figure 2-16, two different reference waters (boundary and fracture water, Table 2-2) have been prescribed and the extent of the different domains will be controlled by the evolution of the shoreline over time. As topography is prescribed as upper boundary, these 3D models enable a detailed analysis of processes occurring in the biosphere.

As chloride does not undergo chemical reactions, its evolution can be used to follow the hydrological patterns of the site. As shown in Figure 4-1, the model provides a precise visualization of chemical changes occurred in the vicinity of the repository and at repository depth. In addition, specific information can be obtained at each point of the model for representing the spatial and temporal evolution of modelled parameters (Figure 4-2a and b, respectively). An abrupt change in chloride concentrations is observed after 3500 AD when meteoric waters arrive at repository depth. This fact is clearly observed analysing the evolution of chloride concentration with time along the A-A′ profile crossing the SFR repositories (Figure 4-2a) and, more specifically, at an observation point located in the repository (Figure 4-2b)(see details in Figure 4-1b). Results previously obtained with the FASTREACT approach (Román-Ross et al. 2014) computed this change in salinity at repository depth in a shorter period (after 2800 AD) due to conceptual simplifications linked to 1D transport simulations. In terms of salinity attenuation, the effect of matrix diffusion is clearly appreciated by comparing simulations run with and without reactive matrix in Figure 4-2 (a, b). Due to conservative behaviour of chloride, the computed results for the Base Case and the Variant Case are identical. Given the parameterization of the reactive rock matrix considered in our model, the attenuation of salinity changes produced by the reactive rock matrix could be overestimated. More realistic values for chloride concentrations should be comprised between the values reported for simulations with and without reactive matrix.

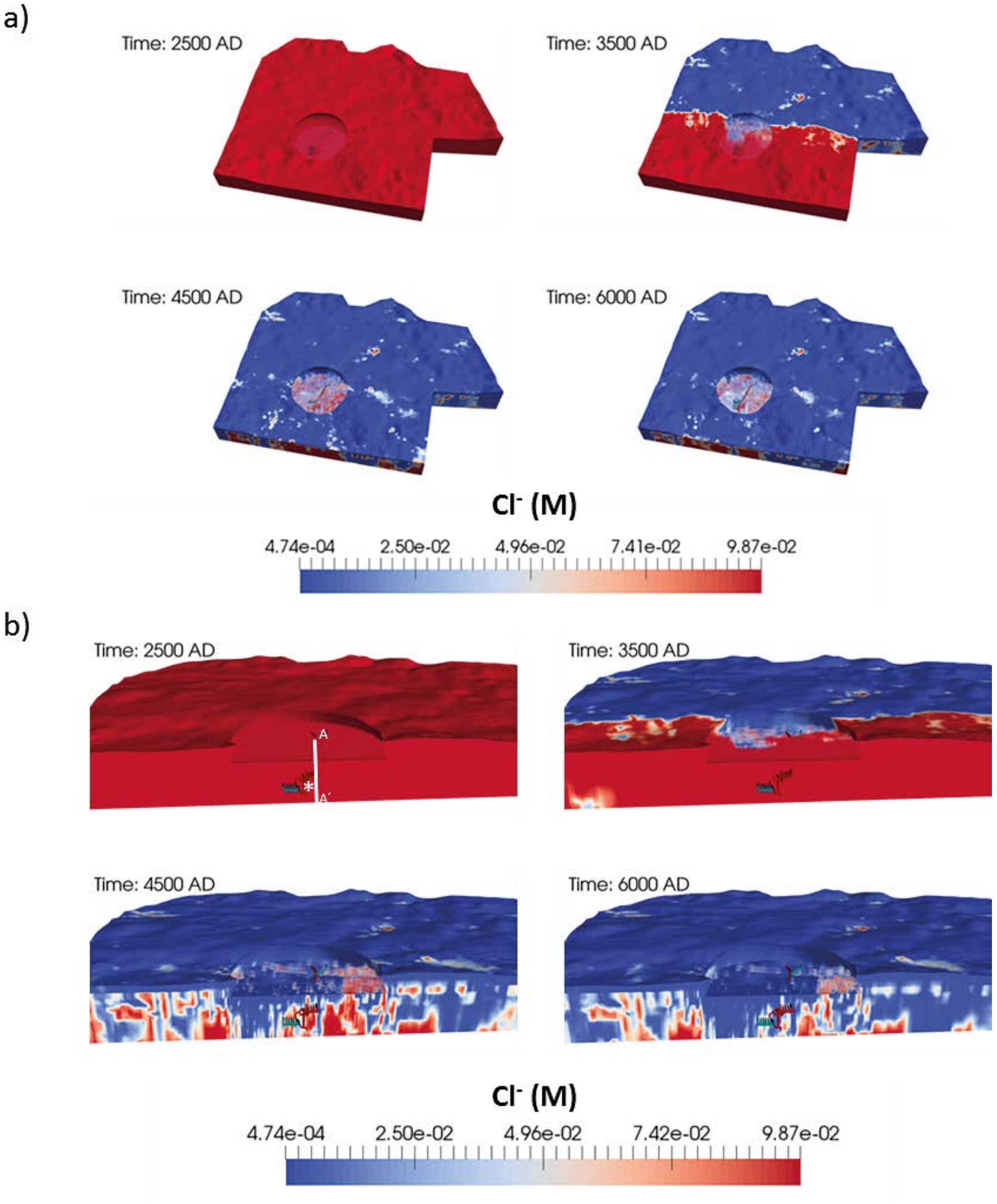
a)
Time: 2500 AD
Time: 3500 AD
Time: 4500 AD
Time: 6000 AD
Cl⁻ (M)
4.74e-04
2.50e-02
4.96e-02
7.41e-02
9.87e-02
b)
Time: 2500 AD
A
*
A´
Time: 3500 AD
Time: 4500 AD
Time: 6000 AD
Cl⁻ (M)
4.74e-04
2.50e-02
4.96e-02
7.42e-02
9.87e-02

Figure 4-1. *Top and cross-sectional views of chloride concentration (Base Case and Variant Case with reactive matrix). (*): Observation point. A-A´: Observation profile.*

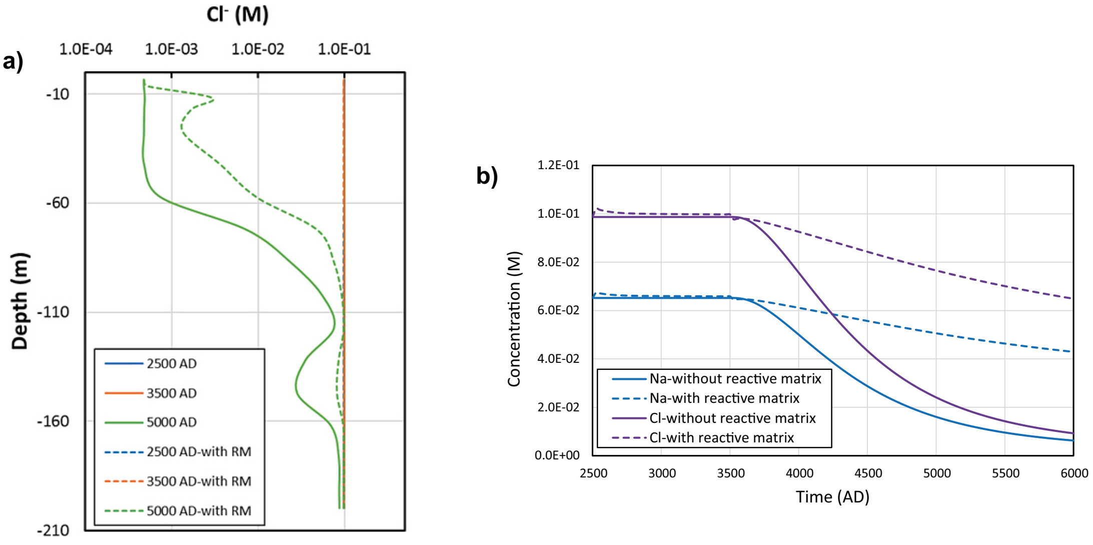

Figure 4-2. *a) Chloride concentration vs elevation for the observation profile A-A´(Base and Variant cases), b) Cl and Na evolution with time computed at the observation point. Please note that the results obtained at 2500 and 3500 AD in the left figure are overlapped. Results obtained for the Base and the Variant case are identical as Cl behave conservatively.*

Other than hydrological conditions, mainly controlled by infiltration processes, the non-conservative chemical constituents will be modified on their reactivity depending on the fracture filling minerals and the interactions with the rock matrix. Figure 4-3 shows the distribution of pH and pe values on cross-sectional views computed at different times for cases with and without reactive matrix. In general terms, the pH values range between 7.2 and 8. These values agrees well with those previously reported (Román-Ross et al. 2014, Auqué et al. 2013). The progressive increase of the values observed in the upper part of the profile (Figure 4-4a), is a consequence of calcite dissolution induced by diluted infiltrating waters. As observed for chloride, rock matrix processes smooth out pH and pe changes. Slight differences are computed for the Base and the Variant cases as calcite controls pH conditions in both run cases (Figure 4-4a, c).

The evolution of redox conditions at repository depth displays permanent anoxic conditions over the computed time span. The differences observed between the two geochemical models are due to the initial geochemical constraints, equilibrium conditions with hematite or FeS(am) are imposed for the Base Case and the Variant Case, respectively (Figure 4-4b, d). The computed values are in the range of pe values reported in Román-Ross et al. (2014) at repository depth (−3 to −4.3). These results indicate that redox conditions, now prevailing at repository depth, will remain over the whole simulation period. During the temperate period, the repository will be increasingly affected by more diluted water that will dissolve calcite and hematite/FeS(am). However, the pH and Eh values will slightly change controlled by these geochemical processes.

The evolution of major cations (Ca, Mg, Na, K) follow a similar trend as chloride (Figure 4-5). Due to lack of reactivity, a piston effect is observed due to water advection for chloride and Na in the models without reactive matrix (Figure 4-2b). The same attenuation observed for chloride is computed for Na concentrations when reactive rock matrix is considered. As cation exchange reactions are not included in this model, changes in the major cation concentrations will be controlled by hydrological conditions (dilution with infiltrating meteoric waters), interaction with the fracture filling minerals (only for Ca), and diffusion processes in the rock matrix.

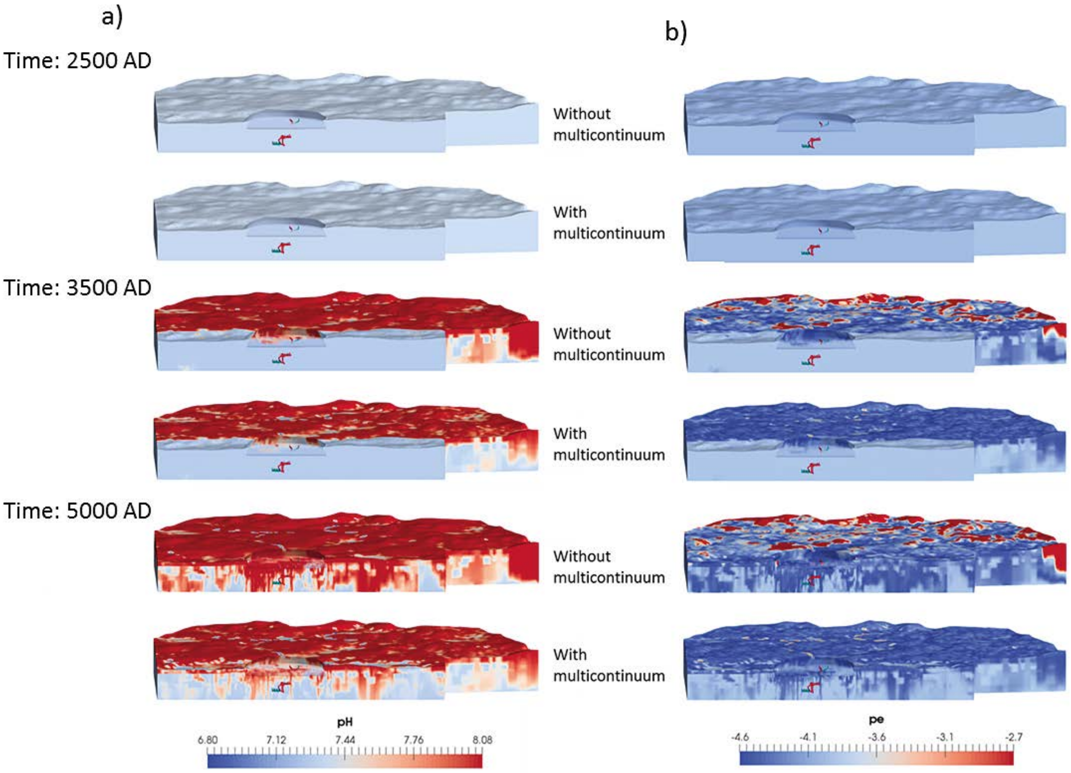
a)
b)
Time: 2500 AD
Without multicontinuum
With multicontinuum
Time: 3500 AD
Without multicontinuum
With multicontinuum
Time: 5000 AD
Without multicontinuum
With multicontinuum
pH
6.80
7.12
7.44
7.76
8.08
pe
-4.6
-4.1
-3.6
-3.1
-2.7

Figure 4-3. *Cross-sectional views of the temporal evolution of pH and pe values computed at different times (Base Case).*

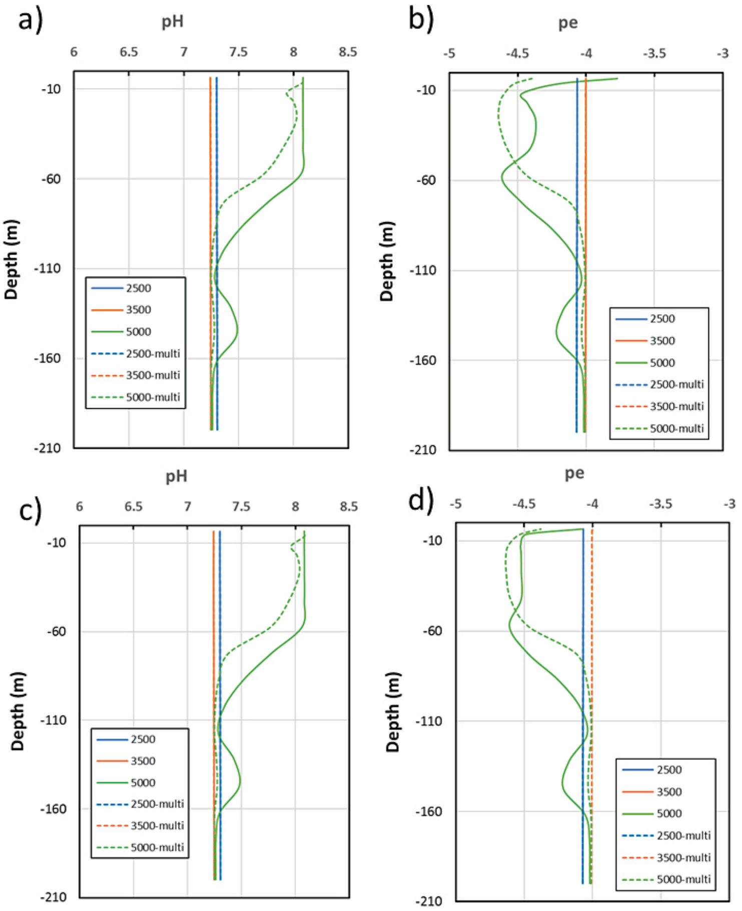

Figure 4-4. *pH and pe values computed in the profile A-A´(Figure 4-1) for the Base Case (a and b) and the Variant Case (c and d). Please note that the results obtained at 2500 and 3500 AD are overlapped.*

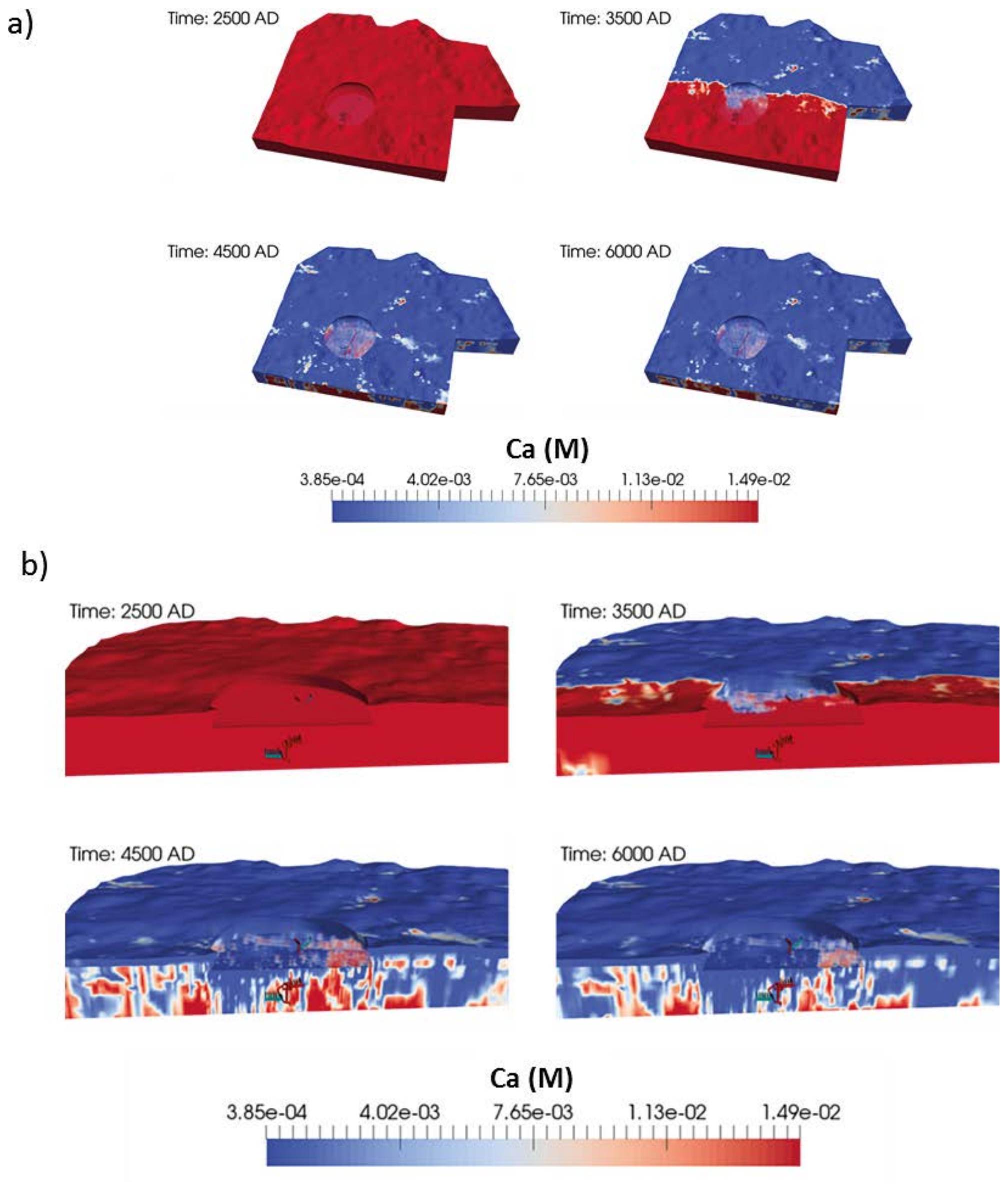

Figure 4-5. *Top and cross-sectional views of Ca concentrations computed at different times.*

Other than initial concentrations prescribed in the fracture and meteoric waters, Mg and K are supplied by biotite dissolution in the rock matrix. It is worth noting that the models run with reactive rock matrix simulate the combined effect of dilution by infiltrating meteoric waters, attenuation by rock matrix effects and cation inputs provided by biotite dissolution (Figure 4-6a, b). Cation inputs from the rock matrix to fracture groundwaters are well observed in Figure 4-6b before the arrival of meteoric waters at repository depth.

In the case of calcium, in addition to matrix-diffusion attenuation and dilution induced by meteoric waters, calcium concentrations are controlled by solution equilibration with calcite present in the fracture fillings (Figure 4-5, Figure 4-6a). The concentrations reported for major cations computed with FASTREACT (Román-Ross et al. 2014), are similar to those obtained with the 3D models run without reactive rock matrix.

Similar to Mg and K behaviour, Al and SiO_2(aq) are controlled by hydrological conditions and chemical exchanges with the rock matrix. Figure 4-7 illustrates the results of these interactions. In the case of dissolved silica (Figure 4-7a) the concentrations increase while fracture water is in contact with the rock matrix. Once the diluted waters arrived, the contents decrease but they remain in the same order of magnitude (in M). A different behaviour is observed for Al; as the initial concentrations are low, the effect of matrix contribution is more clearly evidenced. Even during the infiltration of meteoric waters, aluminium concentrations are higher than those prescribed in the reference waters. It is important to mention that no precipitation of secondary minerals containing Al is considered in our models.

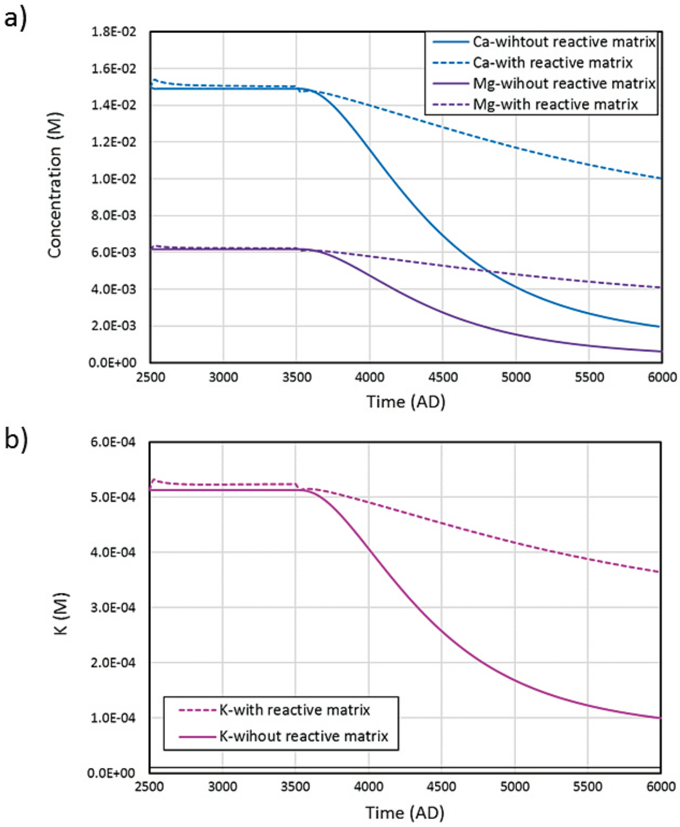

***Figure 4-6.** Evolution of Ca, Mg and K concentration at the observation point defined in Figure 4-1. The computed results for the Base and Variant cases are identical as Ca, Mg and K are controlled by the same processes.*

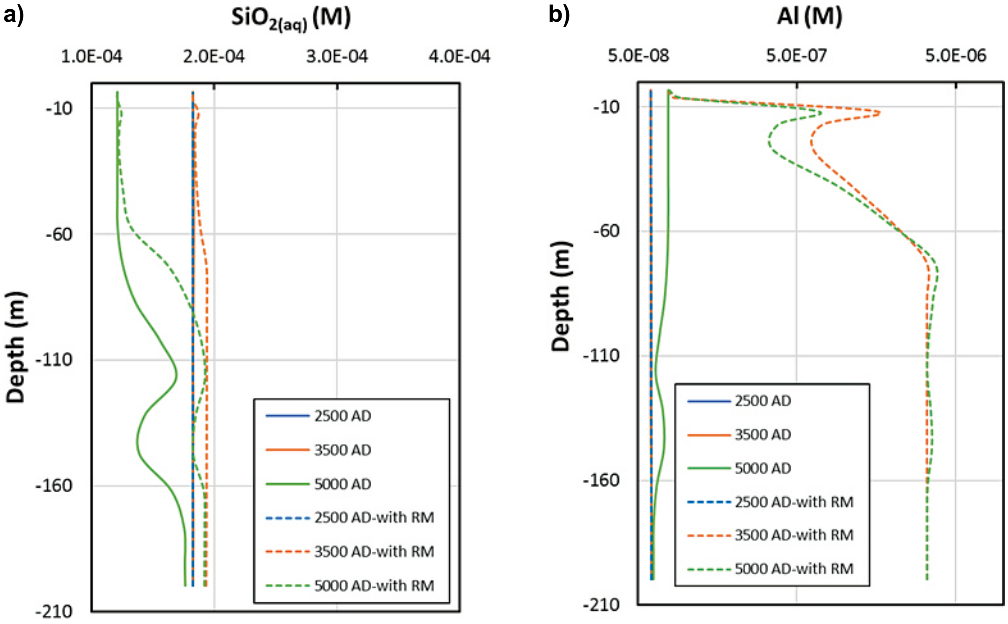

***Figure 4-7.** Silica (a) and Al (b) concentrations computed in the A-A′ profile from the surface down to repository depth. Please note that the results obtained at 2500 are overlapped. The computed results for the Base and Variant cases are identical as $SiO_2(aq)$ and Al are controlled by the same processes.*

Finally, due to Fe concentrations are controlled by dissolution/precipitation of solid phases (hematite or FeS(am)) in the fracture domain, its evolution will depend on the considered geochemical case. Figure 4-8 display the results obtained for the Base Case while Figure 4-9a and b illustrate a comparative analysis for both geochemical models. Higher Fe^{2+} concentrations have been calculated in fracture waters under equilibrium conditions with hematite (a) with respect to those equilibrated with FeS(am) (Figure 4-9b). Anoxic conditions prevent the oxidation of Fe^{2+} to Fe^{3+} and, in turn, the uptake of Fe *via* hematite precipitation. In contrast, precipitation of FeS(am) is an efficient sink of Fe^{2+} provided by the kinetic dissolution of biotite in the rock matrix.

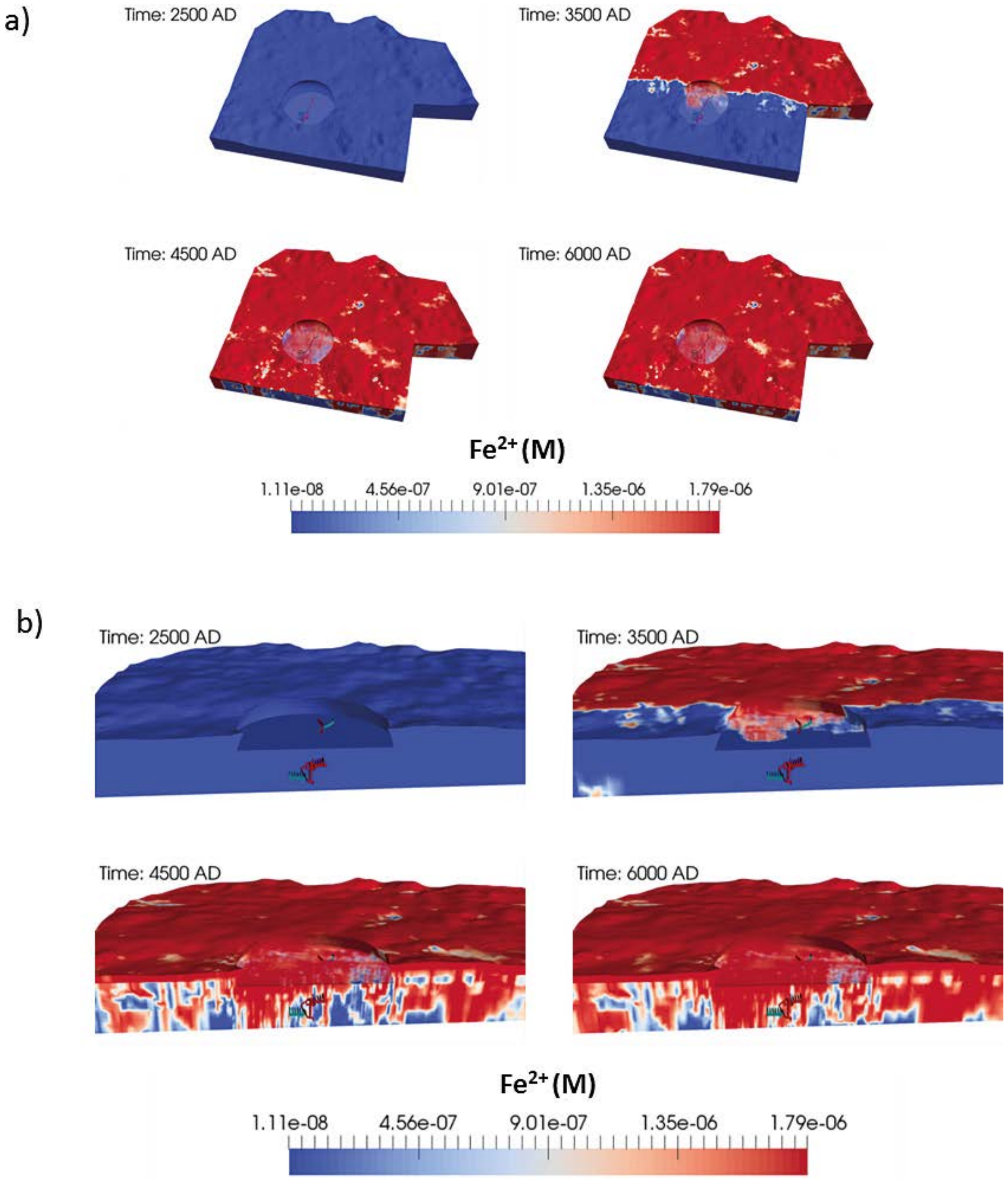
a)
Time: 2500 AD
Time: 3500 AD
Time: 4500 AD
Time: 6000 AD
Fe2+ (M)
1.11e-08
4.56e-07
9.01e-07
1.35e-06
1.79e-06
b)
Time: 2500 AD
Time: 3500 AD
Time: 4500 AD
Time: 6000 AD
Fe2+ (M)
1.11e-08
4.56e-07
9.01e-07
1.35e-06
1.79e-06

Figure 4-8. *Top and cross-sectional views of Fe^{2+} concentrations computed at different times for the Base Case.*

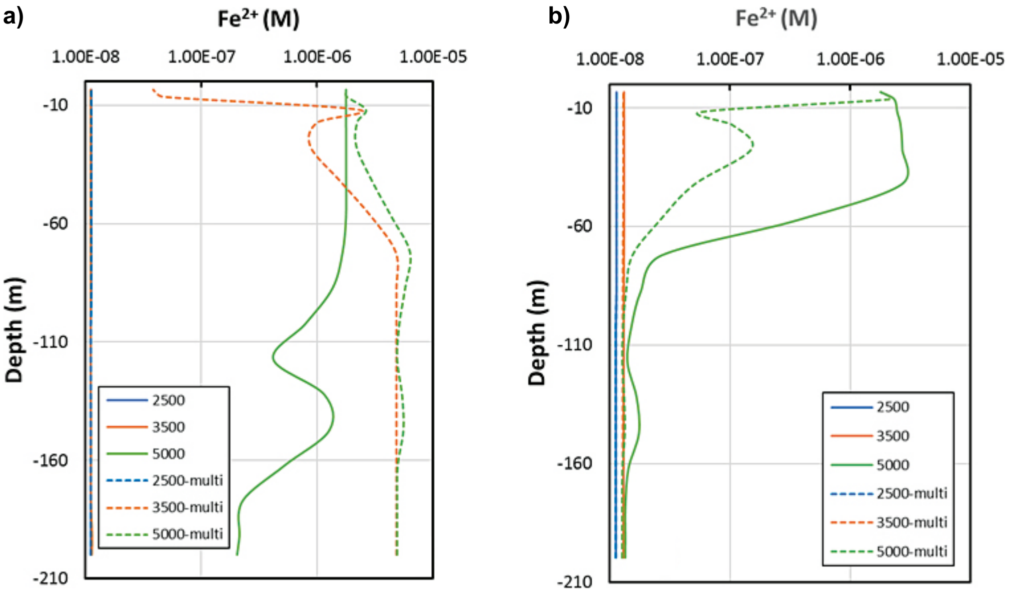

Figure 4-9. *Fe^{2+} concentrations computed for a) Base Case and b) Variant Case for the profile A-A′ from the surface down to repository depth. Please note that the results obtained at 2500 AD are overlapped.*

All these results support the fact that rock matrix should be included in the hydrogeochemical model. Chemical interactions with this reactive domain could attenuate sharp changes in the composition of fracture groundwaters in contact with reactive barrier. However, an adequate parameterization, based on experimental data and well adapted to the specific geologic case, is needed to reproduce the natural system.

A full 3D model is now available to simulate advection and diffusion processes coupled to chemical reactions occurring in the rock matrix and fracture fillings in the SFR geological environment. The model is able to reproduce the geochemical cases defined in a previous study (Román-Ross et al. 2014) adding a large improvement in visualization and computing performance.

5 Concluding remarks and further work

A 3D reactive transport model was developed for the SFR repository including a reactive rock matrix. From a conceptual point of view, geosphere surrounding the SFR repositories was considered as an upscaled equivalent continuous porous medium (ECPM). The heterogeneous properties (i.e. the permeability field and pressure boundary conditions) of this ECPM were computed by DarcyTools and converted to PFLOTRAN using iDP. The implementation of the multicontinuum approach allowed a flexible discretisation of the reactive rock matrix. By including this approach in a 3D model, the interaction between the flowing water in fractures and the porous rock matrix was quantified and compared with a model without reactive matrix.

The results validate iDP (interface DarcyTools-PFLOTRAN) as a powerful tool for modelling hydrogeological and hydrogeochemical processes in the geosphere. One of the main goals achieved by this study is the improvement of computational efficiency applied to a full coupled reactive transport model able to simulate the evolution of groundwater composition in the geosphere surrounding the SFR repositories.

The numerical simulations reproduce the interactions between the fracture groundwater and the rock matrix taking into account the ongoing shoreline displacement and the increasing influence of altered meteoric water over time (from 2500 AD to 6000 AD).

The 3D reactive transport calculations have been run for the two geochemical cases defined for previous models performed with FASTREACT (Román-Ross et al. 2014). The Base Case assumes local equilibrium conditions with calcite/hematite and the alternative geochemical case (Variant Case) has been computed in chemical equilibrium with calcite/amorphous iron monosulphide (FeS(am)). Biotite is assumed to kinetically dissolve in the rock matrix providing Fe^{2+} by diffusion to the fracture groundwater. The 3D model integrates the mutual interdependence of flow and groundwater chemical processes occurring in the fracture domain.

The results show very stable pH conditions for both cases with and without reactive matrix with values ranging between 7.2 and 8. Permanent anoxic conditions were computed over the computed time span. The differences observed between the two geochemical models (Base Case and the Variant Case) are due to the initial geochemical constraints, equilibrium conditions with hematite or amorphous iron monosulphide (FeS(am)), respectively. As observed for chloride, rock matrix processes smooth out pH and pe changes. The effect of reactive rock matrix is clearly evidenced in the temporal/spatial evolution of Fe^{2+}. These results highlight the central role of rock matrix on the evolution of the chemical composition of fracture groundwaters.

The compared results show a good agreement between the FASTREACT results and the new ones computed without reactive matrix. The simulations show that the rock matrix processes have a relevant role in the attenuation of abrupt chemical changes and should be included in the geochemical models. However, a good parameterization of this very heterogeneous domain is strongly dependent on the available characterization studies.

The results computed provide an excellent visualization of solute chemical evolution by means of selected top and cross-sectional views. In addition, the statistical evolution of hydrochemical parameters can be obtained in space and time at each cell of the model.

Coupled reactive transport calculations are now feasible at site scale for the SFR repositories computing hydrogeological and hydrogeochemical processes in a site descriptive model that also integrates the topography of the site. These models can be used as a base model for implementing more complex applications in the future.

iDP has the capability to model coupled processes to simulate different scenarios in an ever-wider range of scales in space and time with a high degree of both detail and complexity. Future application could integrate radionuclide transport, interactions with the reactive barriers or processes occurring in the biosphere.

References

SKB's (Svensk Kärnbränslehantering AB) publications can be found at www.skb.com/publications.

Ahrens J, Geveci B, Law C, 2005. ParaView: an end-user tool for large data visualization. In Hansen C D, Johnson C R (eds). Visualization handbook. Amsterdam: Elsevier, 717–731.

Auqué L F, Gimeno M J, Acero P, Gómez J, 2013. Compositions of groundwater for SFR and its extension, during different climate cases, SR-PSU. SKB R-13-16, Svensk Kärnbränslehantering AB.

Crawford J, 2008. Bedrock transport properties Forsmark. Site descriptive modelling SDM-Site Forsmark. SKB R-08-48, Svensk Kärnbränslehantering AB.

Curtis, P, Markström I, Petersson J, Triumf C-A, Isaksson H, Mattson H, 2011. Site investigation SFR, Bedrock geology, SKB R-10-49, Svensk Kärnbränslehantering AB.

de Hoog, F R, Knight, J H and A. N. Stokes, A N, 1982. An improved method for numerical inversion of Laplace transforms. SIAM Journal on Scientific and Statistical Computing 3, 357–366.

de Marsily G, 1986. Quantitative hydrogeology: groundwater hydrology for engineers. Orlando, FL: Academic Press.

Eaton J W, Bateman D, Hauberg S, Wehbring R, 2014. GNU Octave version 3.8.1 manual: a high-level interactive language for numerical computations. CreateSpace Independent Publishing Platform. Available at: http://www.gnu.org/software/octave/doc/interpreter (Octave 3.8.1 Released (gnu.org) [07 Mar 2014]

Freeze R A, Cherry J A, 1979. Groundwater. Englewood Cliffs, NJ: Prentice Hall.

Hammond G E, Lichtner P C, Mills R T, 2014. Evaluating the performance of parallel subsurface simulators: An illustrative example with PFLOTRAN. Water Resources Research 50, 208–228.

Hollenbeck K J, 1998. INVLAP.M: A Matlab Function for Numerical Inversion of Laplace Transforms by the de Hoog Algorithm. Available at: https://web.archive.org/web/20010318022450/http://www.isva.dtu.dk/staff/karl/invlap.htm [18 March 2001]

Iraola A, 2015. Interface between GiD and PFLOTRAN (iGP): development and application. Master thesis. Universitat Autònoma de Barcelona, Spain.

Iraola A, Trinchero P, Karra S, Molinero J, 2019. Assessing dual continuum method for multicomponent reactive transport. Computers & Geosciences 130, 11–19.

Joyce S, Applegate D, Appleyard P, Gordon A, Heath T, Hunter F, Hoek J, Jackson P, Swan D, Woollard H, 2015. Groundwater flow and reactive transport modelling in ConnectFlow. SKB R-14-19, Svensk Kärnbränslehantering AB.

Lichtner P C, 2000. Critique of dual continuum formulations of multicomponent reactive transport in fractured porous media. In Faybishenko B, Witherspoon P A, Benson S M (eds). Dynamics of fluids in fractured rock. American Geophysical Union, 281–298.

Lichtner G E, Hammond C, Lu S, Karra G, Bisht B, Andre R, Mills, J Kumar, 2013. PFLOTRAN User Manual, Technical report. Available at: http://www.pflotran.org [7 August 2013]

Lichtner P, Hammond G, Lu C, Karra S, Bisht G, Andre B, Mills R, Kumar J, 2015. PFLOTRAN user manual: A massively parallel reactive flow and transport model for describing surface and subsurface processes. Report LA-UR-15-20403, Los Alamos National Laboratory, USA.

Molinero J, Trinchero P, de Vries L M, Ebrahimi H, Svensson U, 2016. The BRIDGE Project. Development, testing and application of a high performance computing framework for reactive transport modelling in crystalline rocks (iDP). SKB R-15-17, Svensk Kärnbränslehantering AB.

Nilsson A-C, Tullborg E-L, Smellie J, Gimeno M J, Gómez J B, Auqué L F, Sandström B, Pedersen K, 2011. SFR site investigation. Bedrock hydrogeochemistry. SKB R-11-06, Svensk Kärnbränslehantering AB.

Palandri J L, Kharaka Y K, 2004. A compilation of rate parameters of water-mineral interaction kinetics for application to geochemical modeling. Open File Report 2004-1068, U.S. Geological Survey.

Román-Ross G, Trinchero P, Maia F, Molinero J, 2014. Hydrogeochemical modelling and evolution of the groundwater types and processes in geosphere of SFR, SR-PSU. SKB R-13-30, Svensk Kärnbränslehantering AB.

Salas J, Gimeno M J, Auqué L F, Molinero J, Gómez J, Juárez I, 2010. SR-Site – hydrogeochemical evolution of the Forsmark site. SKB TR-10-58, Svensk Kärnbränslehantering AB.

Sandström B, Tullborg E-L, Sidborn M, 2014. Iron hydroxide occurrence and redox capacity in bedrock fractures in the vicinity of SFR. SKB R-12-11, Svensk Kärnbränslehantering AB.

Shapiro A M, Cvetkovic V D, 1988. Stochastic analysis of solute arrival time in heterogeneous porous media. Water Resources Research 24, 1711–1718.

Sidborn M, Sandström B, Tullborg E-L, Salas J, Maia F, Delos A, Molinero J, Hallbeck L, Pedersen K, 2010. SR-Site: Oxygen ingress in the rock at Forsmark during a glacial cycle. SKB TR-10-57, Svensk Kärnbränslehantering AB.

Sidborn M, Marsic N, Crawford J, Joyce S, Hartley L, Idiart A, de Vries L M, Maia F, Molinero J, Svensson U, Vidstrand P, Alexander R, 2014. Potential alkaline conditions for deposition holes of a repository in Forsmark as a consequence of OPC grouting. Revised final report after review. SKB R-12-17, Svensk Kärnbränslehantering AB.

SKB 2010. Data report for the safety assessment SR-Site. SKB TR-10-52, Svensk Kärnbränslehantering AB.

SKB, 2014. Miljökonsekvensbeskrivning. Utbyggnad och fortsatt drift av SFR, Svensk Kärnbränslehantering AB. (In Swedish.)

Svensson U, Ferry M, Kuylenstierna H-O, 2010. DarcyTools version 3.4 – concepts, methods and equations. SKB R-07-38, Svensk Kärnbränslehantering AB.

Tang D H, Frind E O, Sudicky E A, 1981. Contaminant transport in fractured porous media: Analytical solution for a single fracture. Water Resources Research 17, 555–564.

Trinchero P, Molinero J, Román-Ross G, 2014. FASTREACT – A streamline-based approach for the solution of multicomponent reactive transport problems. SKB R-10-45, Svensk Kärnbränslehantering AB.

Trinchero P, Puigdomenech I, Molinero J, Ebrahimi H, Gyllingb B, Svensson U, Bosbach D, Deissmann G, 2017. Continuum-based DFN-consistent numerical framework for the simulation of oxygen infiltration into fractured crystalline rocks. Journal of Contaminant Hydrology 200, 60–69.

Appendix

Table A-1. identification of model files delivered to SKB.

Variable	Description	Reference file	PFLOTRAN files
Topography surface	The variable *HSD_surface* comes from the DarcyTools model (2500 AD)	*RUN_2500AD_to_AMPHOS.zip*	*regions.h5*
Permeability (x-component)	*PermX.rof* file generated when running the DarcyTools model (2500 AD)	*RUN_2500AD_to_AMPHOS.zip*	*permeability_*.h5*
Permeability (y-component)	*PermY.rof* file generated when running the DarcyTools model (2500 AD)	*RUN_2500AD_to_AMPHOS.zip*	
Permeability (z-component)	*PermZ.rof* file generated when running the DarcyTools model (2500 AD)	*RUN_2500AD_to_AMPHOS.zip*	
Pressure field (2500 AD)	*pressure.rof* file generated when running the DarcyTools model (2500 AD)	*RUN_2500AD_to_AMPHOS.zip*	*pressure_bottom_*.h5* *pressure_top_*.h5* *pressure_*.h5* *(for initialization)*
Pressure field (3500 AD)	*pressure.rof* file generated when running the DarcyTools model (3500 AD)	*RUN_3500AD_to_AMPHOS.zip*	
Pressure field (5000 AD)	*pressure.rof* file generated when running the DarcyTools model (5000 AD)	*RUN_5000AD_to_AMPHOS.zip*	
SFR1 layout files (postprocess)	Tecplot file containing the layout of the SFR1 repository	*SFR1_to_Amphos.lpk*	-
SFR3 layout files (postprocess)	Tecplot file containing the layout of the SFR3 repository	*SFR3_to_Amphos.lpk*	-

Table A-2. List of output files.

ID	File	Description
0	Simulation split in three parts: 1. BC_2500-3500_convergence2.h5 2. BC_3500-5000.h5 3. BC_5000-6000.h5	Base case (2015 model)
1	Simulation split in three parts: 1. Chemistry_2500-3500.h5 2. Chemistry_3500-5000.h5 3. Chemistry_5000-6000B.h5	Variant case (2015 model)
2	input_BC_unsaturated_nomulti.h5	Base case/unsaturated (topography model)
3	input_VC_unsaturated_nomulti_B.h5	Variant case/unsaturated (topography model)
4	input_BC_saturated_nomulti.h5	Base case/saturated (topography model)
5	input_VC_saturated_nomulti_B.h5	Variant case/saturated (topography model)
6	Input_BC_saturated_multi.h5	Base case with multicontinuum/saturated (topography model)
7	Input_VC_saturated_multi_141216_C.h5	Variant case with multicontinuum/saturated (topography model)

All the hdf5 output files need the corresponding *.xmf* set of files (i.e. one file for each timestep). When using Paraview to visualize the results, one needs to open the set of *.xmf* files (the corresponding hdf5 file is loaded automatically).

Arkitektkopia AB, Bromma, 2024

SKB is responsible for managing spent nuclear fuel and radioactive waste produced by the Swedish nuclear power plants such that man and the environment are protected in the near and distant future.

skb.se

SVENSK KÄRNBRÄNSLEHANTERING